








ORIGINAL RESEARCH

# Neurovascular Uncoupling Is Linked to Microcirculatory Dysfunction in Regions Outside the Ischemic Core Following Ischemic Stroke

Christian Staehr , MD, PhD; John T. Giblin , PhD; Eugenio Gutiérrez-Jiménez, PhD; Halvor Ø. Guldbrandsen , MBBS; Jianbo Tang , PhD; Shaun L. Sandow , PhD; David A. Boas , PhD; Vladimir V. Matchkov , DMSc

**BACKGROUND:** Normal brain function depends on the ability of the vasculature to increase blood flow to regions with high metabolic demands. Impaired neurovascular coupling, such as the local hyperemic response to neuronal activity, may contribute to poor neurological outcome after stroke despite successful recanalization, that is, futile recanalization.

**METHODS AND RESULTS:** Mice implanted with chronic cranial windows were trained for awake head-fixation before experiments. One-hour occlusion of the anterior middle cerebral artery branch was induced using single-vessel photothrombosis. Cerebral perfusion and neurovascular coupling were assessed by optical coherence tomography and laser speckle contrast imaging. Capillaries and pericytes were studied in perfusion-fixed tissue by labeling lectin and platelet-derived growth factor receptor  $\beta$ . Arterial occlusion induced multiple spreading depolarizations over 1 hour associated with substantially reduced blood flow in the peri-ischemic cortex. Approximately half of the capillaries in the peri-ischemic area were no longer perfused at the 3- and 24-hour follow-up (45% [95% CI, 33%–58%] and 53% [95% CI, 39%–66%] reduction, respectively;  $P < 0.0001$ ), which was associated with contraction of an equivalent proportion of peri-ischemic capillary pericytes. The capillaries in the peri-ischemic cortex that remained perfused showed increased point prevalence of dynamic flow stalling (0.5% [95% CI, 0.2%–0.7%] at baseline, 5.1% [95% CI, 3.2%–6.5%] and 3.2% [95% CI, 1.1%–5.3%] at 3- and 24-hour follow-up, respectively;  $P = 0.001$ ). Whisker stimulation at the 3- and 24-hour follow-up led to reduced neurovascular coupling responses in the sensory cortex corresponding to the peri-ischemic region compared with that observed at baseline.

**CONCLUSIONS:** Arterial occlusion led to contraction of capillary pericytes and capillary flow stalling in the peri-ischemic cortex. Capillary dysfunction was associated with neurovascular uncoupling. Neurovascular coupling impairment associated with capillary dysfunction may be a mechanism that contributes to futile recanalization. Hence, the results from this study suggest a novel treatment target to improve neurological outcome after stroke.

**Key Words:** capillaries ■ ischemic stroke ■ neurovascular coupling ■ penumbra ■ pericytes

In the central nervous system, there is an accurately balanced coupling between neuronal tissue activity and the function of the supplying vasculature.

Neurovascular coupling ensures a rapidly increased supply of oxygen and nutrition to active brain regions.<sup>1</sup> The communication on which this is dependent is

Correspondence to: Christian Staehr, Department of Biomedicine, Aarhus University Høegh-Guldbergs Gade 10, DK-8000 Aarhus C, Denmark. Email: [chst@biomed.au.dk](mailto:chst@biomed.au.dk)

Supplemental Material is available at <https://www.ahajournals.org/doi/suppl/10.1161/JAHA.123.029527>

This article was sent to Kori S. Zachrisson, MD, MSc, Associate Editor, for review by expert referees, editorial decision, and final disposition.

Preprint posted on bioRxiv August 26, 2022. DOI: <https://doi.org/10.1101/2022.08.26.505245>

For Sources of Funding and Disclosures, see page 13.

© 2023 The Authors. Published on behalf of the American Heart Association, Inc., by Wiley. This is an open access article under the terms of the [Creative Commons Attribution-NonCommercial](https://creativecommons.org/licenses/by-nc/4.0/) License, which permits use, distribution and reproduction in any medium, provided the original work is properly cited and is not used for commercial purposes.

JAHA is available at: [www.ahajournals.org/journal/jaha](http://www.ahajournals.org/journal/jaha)

## RESEARCH PERSPECTIVE

### What Is New?

- The local increase in blood flow in response to neuronal activity, as neurovascular coupling, is impaired after ischemic stroke reperfusion.
- The impaired neurovascular coupling after stroke is associated with capillary dysfunction in peri-ischemic brain regions.
- Capillary dysfunction after stroke is associated with contraction of pericytes and capillary flow stalling.

### What Questions Should Be Addressed Next?

- Future research should clarify whether capillary dysfunction and neurovascular uncoupling are correlated with neurological outcomes in patients with ischemic stroke.
- Identifying pharmacological interventions that target pericyte contraction could improve capillary function and restore neurovascular coupling after stroke.

## Nonstandard Abbreviations and Acronyms

<b>LSCI</b>	laser speckle contrast imaging
<b>MCA</b>	middle cerebral artery
<b>OCT</b>	optical coherence tomography

believed to be transmitted through release of vasoactive substances from the active neuronal tissue, which in turn dilate parenchymal arterioles, increasing blood flow.<sup>2,3</sup> Furthermore, the capillary circulation plays an important role in the modulation of neurovascular coupling. It has been suggested that pericytes associated with cerebral capillaries contain smooth muscle actin and are contractile,<sup>4–6</sup> with the related mechanism preferentially shunting capillary blood flow for specific tissue perfusion.<sup>7</sup> Nevertheless, whether pericytes actively regulate capillary diameter in response to neuronal activity and thus contribute to neurovascular coupling remains controversial.<sup>6–10</sup>

Futile recanalization, as poor neurological outcome despite successful recanalization, is observed in more than 50% of patients with ischemic stroke.<sup>11–13</sup> The mechanism behind futile recanalization remains uncertain. Impaired neurovascular coupling, which may contribute to neurological deterioration over time,<sup>9</sup> has been reported in patients following ischemic stroke.<sup>14–16</sup> Importantly, these studies suggest that reduced neurovascular coupling is also observed in brain regions apart from the ischemic core. Hence, it has been

speculated that impaired neurovascular responses in patients with stroke were caused by a preexisting diffuse vascular pathology.<sup>14–17</sup> The present study aimed to address this unanswered question by comparing neurovascular responses in the peri-ischemic area before stroke and after ischemia reperfusion. It was hypothesized that impaired neurovascular coupling in the peri-ischemic area is caused by disrupted capillary microcirculation. The hypothesis was tested in an awake mouse model of stroke by performing a thorough characterization of cerebrovascular function in the peri-ischemic area before, during, and after cerebral ischemia. By studying the dynamic changes in cerebral blood flow during arterial occlusion and after reperfusion, a unique mechanistic insight into the cerebrovascular events in ischemic stroke was obtained. With state-of-the-art imaging techniques, a mechanism that may underlie widespread neurovascular uncoupling contributing to futile recanalization in patients with stroke was uncovered.

## METHODS

The data that support the findings of this study are available from the corresponding author upon reasonable request. All experiments were in accordance with institutional guidelines and were approved by the Institutional Animal Care and Use Committees at Boston University. Experiments were conducted following the *Care and Use of Laboratory Animals* guidelines and reported in accordance with the Animal Research: Reporting in Vivo Experiments guidelines. Female C57BL/6 mice (Jackson Laboratory, Bar Harbor, ME) were used (Table S1). Only females were included because of their calm behavior during awake imaging, easier housing after the implementation of chronic cranial window, and to prevent sex-dependent variability because estrogen and testosterone affect the vascular function,<sup>18</sup> binding of blood cells to the endothelium,<sup>19</sup> and infarct size after experimental stroke.<sup>20</sup> The experimental group size was estimated based on a power calculation suggesting 6 to 7 mice to detect a statistical difference ( $P < 0.05$ ) in neurovascular coupling responses at baseline versus 3-hour follow-up with the power of 0.8 (80% chance to determine 5 percentage points difference). Mice were 18 weeks old when chronic cranial windows were prepared and 24 to 26 weeks old when the stroke-reperfusion protocol commenced. Mice were housed under a 12:12 light/dark cycle, and food and water were provided ad libitum.

## Surgical Procedure and Habituation Training

Four hours before the surgical procedure, 4.8 mg/kg dexamethasone (4 mg/mL) was administered IP to

minimize cerebral tissue swelling during surgery. Two hours before anesthesia, 0.5 mg/kg slow-release buprenorphine (1 mg/mL) and 5 mg/kg meloxicam (5 mg/mL in 0.9% NaCl) were injected subcutaneously. Body temperature was maintained at 37 °C during surgery and controlled with a rectal probe. Surgery was performed under isoflurane anesthesia (2%–3% induction, 1%–2% maintenance, in 1 L/min oxygen). Craniotomy over 1 hemisphere was performed. Dura mater was left intact. The brain surface was covered with a piece of curved glass (LabMaker, Berlin, Germany) that was shaped to fit the cranial window and sealed with dental acrylic and instant super adhesive glue. A circular aluminum bar was attached to the skull around the cranial window for head fixation during experiments. Meloxicam (5 mg/kg) was administered every 24 hours 3 days after surgery. Mice were allowed to recover from surgery for at least 14 days before starting habituation training. Mice were gradually habituated to longer periods of head-fixation over 7 training sessions starting at a duration of 10 minutes and ending at 1.5 hours. While head-fixed, mice were able to readjust body position. After each habituation session, mice were rewarded with sweetened milk.

### Photothrombosis

Single-vessel photothrombosis was performed as previous<sup>21</sup> to occlude the anterior middle cerebral artery (MCA) branch while causing minimal damage to the surrounding parenchyma (Figure 1A and 1B). Under brief isoflurane sedation (1% in 1 L/min oxygen), 100  $\mu$ L of Rose Bengal (15 mg/mL in 0.9% NaCl; Sigma Aldrich, St. Louis, MO) was injected retro-orbitally. Rose Bengal is activated with green light. Therefore, blue light was used to visualize the vasculature with a multispectral camera and thus did not lead to photoactivation. The green laser diode (520 nm) was tuned to a postobjective power of 0.6 mW and focused to a diameter of 6  $\mu$ m. Real-time laser speckle contrast imaging (LSCI) was used to detect when the target vessel was occluded. When no blood flow was observed, the green laser was left on for another 2 minutes and then turned off. In the case of spontaneous reperfusion during the 1-hour occlusion, the green laser was turned on until the vessel was occluded again. Collateral blood flow supply can prevent single-vessel occlusion from having a significant reduction in blood flow in mice and thus resulting in the formation of an ischemic core.<sup>21,22</sup> Therefore, a collateral artery was targeted if it appeared after occlusion and supplied the perfusion field for the occluded MCA branch. Collateral blood supply was targeted in 50% of the mice. All measurements were acquired longitudinally, implying that cerebral blood flow and arterial diameter were measured from the same subject over time.

### Optical Coherence Tomography

A spectral-domain optical coherence tomography (OCT; Telesto III, Thorlabs, Newton, NJ) system with a 1310 nm center wavelength and a bandwidth of 170 nm was used. The axial spatial resolution was 3.5  $\mu$ m in the brain, which was determined by the light source. A  $\times 10$  objective NA=0.28 (Mitutoyo, Kawasaki, Japan) was used to image the cerebral microcirculation.<sup>23</sup> The focused beam was adjusted at a depth of around 150 to 200  $\mu$ m, which enabled acquisition of blood flow signal down to  $\sim 300$   $\mu$ m from the brain surface. The blood vessels were imaged with OCT angiography,<sup>24</sup> which detects the intrinsic dynamic contrast of the moving red blood cells by taking the difference of repeated OCT B-scans. A larger 3 $\times$ 3 mm field of view region and a smaller 600 $\times$ 600  $\mu$ m field of view region were obtained at the baseline and at the 3-hour and 24-hour follow-up. The location of the 600 $\times$ 600  $\mu$ m region of interest was based on the supply area of the MCA branch neighboring the occluded anterior MCA branch. Both MCA branches were fed by the same upstream artery. This region of interest was determined at baseline to image the same location at the follow-up time points. For the larger 3 $\times$ 3 mm field of view, 5 angiograms were obtained and averaged. For the smaller 600 $\times$ 600  $\mu$ m field of view, 90 sequential OCT angiograms were obtained over 10 minutes. Maximum intensity projections over a range of 90  $\mu$ m were extracted for analysis in the depth of 210 to 390  $\mu$ m from the brain surface. This range was selected because of the dense capillary network at this depth.

Dynamic capillary flow stalling was defined as sudden intensity drop and thus disappearance of a capillary segment in  $\geq 1$  of the 90 consecutive smaller 600 $\times$ 600  $\mu$ m field of view angiograms. Capillary segments that appeared at any of the 90 angiograms were included when counting perfused capillary segments. Previous analysis of dynamic flow stalling of capillaries with the use of the same approach showed that day-to-day variations between the measurements from the same region of interest were minimal.<sup>23</sup> Counting of capillaries was done manually using ImageJ software (National Institutes of Health, Bethesda, MD).

Phase-resolved Doppler-OCT was recorded with 25 repeated A-lines to assess the axial blood flow velocities of cortical blood vessels penetrating the cortex vertically.<sup>25,26</sup> Phantom validation revealed a lower axial velocity detection limit at  $\sim 0.2$  mm/s; upper detection limit was  $\sim 15$  mm/sec, which depended on the OCT system A-line scan rate. Phase-resolved Doppler-OCT was done in the same region of interest as the smaller field-of-view angiogram. Capillaries with diameters ranging between 3 and 6  $\mu$ m penetrating the cortex in a vertical direction were marked manually for each vessel in a single depth. Vertical capillaries were included regardless

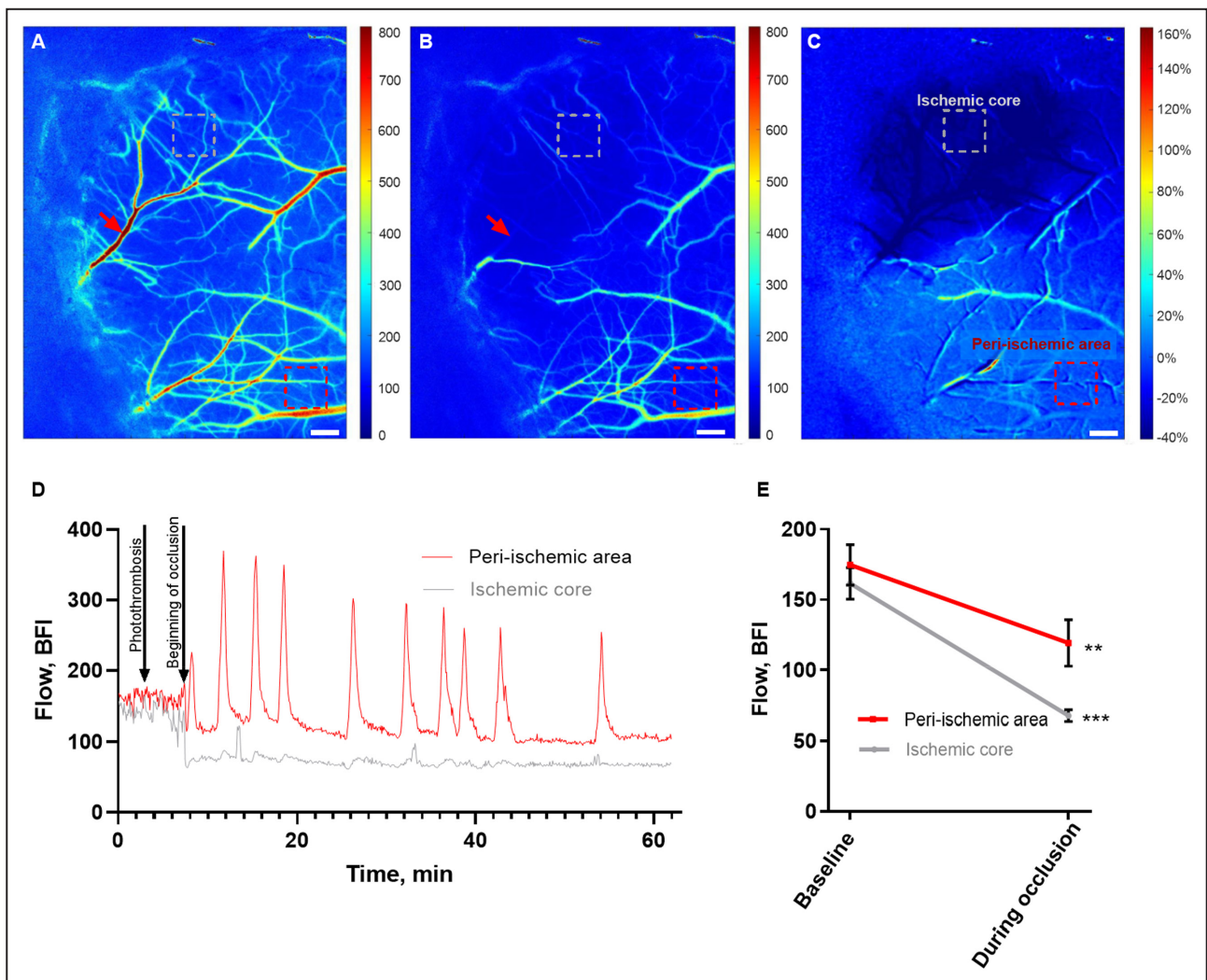


**Figure 1. Cerebral ischemia induced by single-vessel photothrombosis of the middle cerebral artery.** Representative laser speckle contrast images (LSCI) of the affected hemisphere in the awake mouse at baseline (A) and during occlusion of the anterior middle cerebral artery (MCA) branch (B). Red arrows show the focus point for the green laser beam ( $\varnothing=6\ \mu\text{m}$ ) used for photothrombosis of the anterior MCA branch (A and B). C, Image of the ratio of LSCI before vs during the occlusion. Bars,  $300\ \mu\text{m}$ ; dotted boxes indicate the region of interest in the ischemic core (gray) and the peri-ischemic area (red; A–C). D, Representative traces from these 2 regions show the changes in blood flow during the MCA occlusion. E, MCA occlusion was associated with a drop in blood flow in the ischemic core and in the peri-ischemic area. Blood flow during occlusion was compared with baseline in 2 separate 2-tailed paired *t* tests for each of the areas. Error bars=SE. **\*\*** $P<0.01$ , **\*\*\*** $P<0.001$ ;  $n=6$ . BFI indicates blood flow index.

of whether flow direction was ascending or descending; capillaries with descending flow, for example, with a detected velocity of  $-2\ \text{mm/s}$ , were included in the analysis as having flow velocity of  $2\ \text{mm/s}$ . Capillaries were selected over a depth range of  $180$  to  $300\ \mu\text{m}$ . To minimize background noise, a threshold was set to exclude velocities slower than  $0.1\ \text{mm/s}$ . The OCT angiography and phase-resolved Doppler-OCT MATLAB codes are available at <https://github.com/BUNPC/OCTA>.

### Laser Speckle Contrast Imaging and Air-Puff Whisker Stimulation

Coherent near-infrared light was delivered by a laser diode ( $785\ \text{nm}$ , LP785-SAV50, Thorlabs Inc.). The

diode was controlled by current and temperature controllers (LDC210C and TED200C, respectively; Thorlabs Inc.). Backscattered light was recorded using a  $2\times$  lens (TL2X-SAP, Thorlabs Inc.) mounted on a complementary metal oxide semiconductor camera (acA2040-90 $\mu\text{m}$ , Basler AG, Ahrensburg, Germany). A  $650\ \text{nm}$  long pass filter prevented the  $520\ \text{nm}$  photothrombosis laser from affecting the LSCI. The LSCI data were analyzed by applying the commonly used model of arbitrary blood flow index calculated by  $1/K^2$  where  $K$  is contrast.<sup>27</sup> LSCI is generally used to measure the relative change in blood flow, which is mostly independent of the imaging system. However, an absolute blood flow index can be compared within the



same imaging system if the system parameters are held constant.<sup>27–29</sup> By allowing the speckle size to be more than 2 pixels and maintaining all other system parameters constant throughout the study, we were able to maximize this comparison in our system.

Baseline and follow-up recordings were made over 180s with a frame rate of 194 Hz and a resolution of 1024×512 pixels. During the 60-minute occlusion, LSCI frame rate was set to 5 Hz and resolution to 1800×1200 pixels. The pixel size for all LSCI recordings was 3 μm. The LSCI data were processed using temporal speckle contrast analysis, where 25 frames were used to calculate contrast. A segmentation algorithm<sup>30</sup> was used to analyze single-vessel flow velocity as previously described.<sup>31</sup> Arbitrary flow velocity was based on the average laser speckle contrast value in the lumen of the vessel segment.

Whisker stimulation was done using air-puff. Five seconds of whisker stimulation was preceded by 5-second baseline and followed by 20 seconds without stimulation. This 30-second protocol was repeated 20 times, and the relative change in blood flow to each baseline period assessed by LSCI. In whisker stimulation experiments, the frame rate was 40 Hz, and data were processed using spatial speckle contrast analysis to get a high temporal resolution. Custom-made MATLAB scripts used to process and analyze LSCI data are available at <https://github.com/BUNPC/laserSpeckleImaging>.

### Labeling of Capillaries and Pericytes

For structural analyses, mice were perfusion fixed through the left ventricle under 3% isoflurane with 4% formaldehyde in Dulbecco's CaCl<sub>2</sub> and MgCl<sub>2</sub> free PBS. Brains were subsequently postfixed for 24 hours in 4% formaldehyde in PBS at 21 °C and afterwards stored in PBS at 4 °C. The fixed brains were embedded in paraffin and sectioned in 5 μm slices at the level of the peri-ischemic sensory cortex, approximately corresponding to the region of interest for OCT angiography assessment of capillary flow. Sections including both hemispheres were incubated for 16 hours in primary antibody (1:500 rabbit anti-PDGFRβ, #ab32570, Abcam, Cambridge, UK) at 4 °C followed by 2 hours incubation in secondary antibody (1:500 goat anti-rabbit IgG, Alexa Fluor 488, #ab150077, Abcam) at 21 °C. Lipofuscin autofluorescence was reduced using TrueBlack Autofluorescence Quencher (1:20, Biotium, Fremont, CA) for 60 seconds. The whole sections were imaged using Olympus VS120 slide scanner (Olympus, Tokyo, Japan) at ×40 magnification. After imaging the pericytes, the samples were prepared for lectin labeling. Samples were treated for 5 minutes with pepsin (4 mg/mL PBS) at 37 °C before 2-hour lectin incubation at 21 °C (1:100 Lycopersicon Esculentum [Tomato

Lectin, DyLight 649, DL-1178-1 [10 μg/mL], Vector Labs, Newark, CA). Nuclei were stained with 300 nM 4', 6-diamidino-2-phenylindole (DAPI) before mounting. The slide scanning was repeated, and the images with the 3 different labels of the same tissue were registered and overlaid using Control Points Registration in Matlab (ver. R2022a, Natick, MA). Capillary diameter was assessed automatically in ImageJ (National Institutes of Health) using VasoMetrics.<sup>32</sup> Assessment of whether capillaries were associated with a pericyte body was based on whether the capillary had PDGFRβ (platelet-derived growth factor receptor beta) and DAPI-positive cells. The entire capillary segment was included for diameter measurement. Criteria for peri-ischemic capillaries to be included in the analysis were (1) the capillary appeared in the peri-ischemic tissue corresponding to the region of interest where laser speckle and OCT imaging were obtained; and (2) the assessment of contrast was determined automatically by the VasoMetrics.

### Statistical Analysis

MATLAB R2022a and GraphPad Prism software (v.9.3.1) were used for graphing and statistical analyses. Data are summarized as the mean value±SEM of the sample group. Significant differences between means were determined by either 1-way ANOVA with Dunnett's correction for multiple comparisons or 2-way ANOVA with Bonferroni's correction where appropriate. Two separate analyses were conducted to compare the blood flow in the ischemic core and peri-ischemic cortex with their respective baselines. Thus, the blood flow in each area was evaluated in distinct analyses. Mixed-effect analysis with Dunnett's correction was used instead of ANOVA to compare OCT data on MCA diameter because 1 follow-up data point from a single mouse was missing. In the mixed-effect analysis, arterial diameter and time were the fixed effects and subjects were the random effect. A *P* level of <0.05 was considered significant.

## RESULTS

### Arterial Occlusion Resulted in Spreading Depolarizations

With the use of LSCI it was ensured that single-vessel photothrombosis led to 60-minute no-flow in the anterior branch of MCA (Figure 1A and 1B). This outcome was associated with 57±3% drop in perfusion of the downstream cortex (Figure 1C through 1E). Blood flow in the peri-ischemic area corresponding to the whisker sensory cortex was reduced by 33±6% during occlusion (Figure 1E). All 6 mice showed spontaneous reperfusion of the targeted artery within

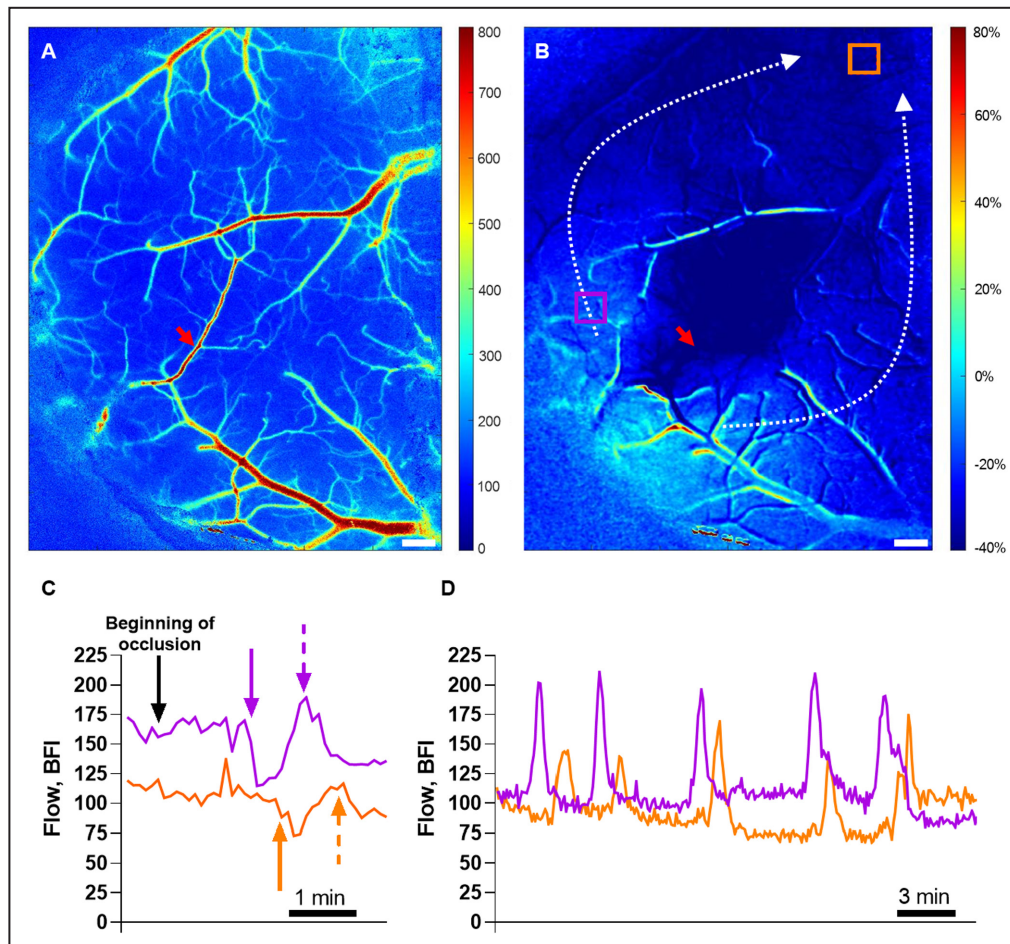


**Figure 2. Spreading depolarizations were elicited by cerebral ischemia.**

**A**, Representative laser speckle contrast image (LSCI) at baseline. **B**, Ratio of LSCI before vs during the occlusion identified the ischemic region. Dotted white arrows show the propagation of spreading depolarizations that were initiated from the lateral part of the penumbral cortex (**B**; see also Video S1). Two regions of interest (ROIs) were placed just outside the ischemic core (violet) and in the peri-ischemic area (orange; **B**). Bars, 300  $\mu$ m; red arrows indicate the photothrombosis focus point (**A**, **B**). Representative traces from these 2 ROIs at the beginning of occlusion (**C**) and 25 to 50 minutes after initiation of the occlusion (**D**). The black arrow indicates the time when the middle cerebral artery occlusion started (**C**). Approximately 2 minutes after the occlusion, the first spreading depolarization propagated. The solid violet and orange arrows show the beginning of the hypoperfusion whereas the dotted arrows indicate the subsequent hyperperfusion followed by sustained hypoperfusion (**C**). During this global hypoperfusion, several spreading depolarizations propagated and were associated with waves of hyperperfusion (**D**). The delayed changes in blood flow in the area corresponding to the orange ROI are caused by spreading depolarization propagation. See Table S2 for details about the spreading depolarizations. BFI indicates blood flow index.

3 hours. Within minutes after onset of the occlusion, spreading depolarizations propagated from the peri-ischemic area to the rest of the hemisphere (Video S1 and Figure 2A and 2B). Spreading depolarizations were observed during occlusion in all 6 mice. On average, 11 spreading depolarizations were observed during the 60-minute occlusion period (Table S2). The propagation velocity of the spreading depolarizations was 3 to 5 mm/min (Table S2). For the first observed spreading depolarization, a period of hypoperfusion preceded a subsequent period of hyperperfusion

followed by sustained hypoperfusion (Video S1 and Figure 2C). The duration of the initial hypoperfusion was shorter than the subsequent hyperperfusion (Table S2). After the first spreading depolarization, blood flow was globally reduced. During this global hypoperfusion, several spreading depolarizations were propagated and associated with waves of hyperperfusion (Figure 2D and Table S2). The initiation of spreading depolarizations was not associated with the photothrombosis laser being on nor with spontaneous reperfusion.

## Reduced Neurovascular Coupling in the Peri-Ischemic Area After Ischemic Stroke

Neurovascular coupling was assessed at baseline before arterial occlusion and at the 3- and 24-hour follow-up. At baseline, 5-second air-puff whisker stimulation was associated with a localized increase in blood flow in the contralateral whisker sensory cortex (Figure 3A and 3B). This neurovascular response was reduced at the 3- and 24-hour follow-up (Figure 3B). Neurovascular coupling was further reduced at the 24-hour follow-up compared with the response observed at the 3-hour follow-up.

## Resting Perfusion of the Peri-Ischemic Cortex was Reduced at the 3-Hour Follow-up but Returned to the Baseline Value After 24 Hours

Results from LSCI (Figure 4A) showed that perfusion of the cortex downstream from the occluded MCA branch remained suppressed at the 3- and 24-hour follow-up (Figure 4B). In the peri-ischemic area, supplied by the neighboring MCA branch of the occluded anterior MCA branch, cortical perfusion was also reduced at the 3-hour follow-up compared with baseline (Figure 4B). At the 24-hour follow-up, perfusion of the peri-ischemic cortex was similar to that observed at baseline.

Blood flow was also assessed in the neighboring MCA branch of the occluded anterior MCA branch (Figure 4A). This neighboring MCA branch supplied the peri-ischemic region of interest. Similar to the observed changes in tissue perfusion of the peri-ischemic area, blood flow in this neighboring artery was reduced during the occlusion and at the 3-hour follow-up but was not statistically different from baseline at the 24-hour follow-up (Figure 4C). The diameter of the neighboring MCA branch was evaluated using absolute values. Although no change from baseline was observed at the 3-hour follow-up, the neighboring MCA branch exhibited vasodilation at the 24-hour follow-up (Figure 4D and 4E).

## Increased Flow Stalling of the Capillary Circulation After Reperfusion in the Peri-Ischemic Area

OCT angiography was obtained in the peri-ischemic cortex (Figure 5A and 5B). Region of interest was located in the same area as for LSCI recordings. The distance from the border of the ischemic core to the closest border of the region of interest was not statistically different at the 2 follow-up time points ( $489 \pm 178 \mu\text{m}$  versus  $407 \pm 169 \mu\text{m}$ , 3- and 24-hour follow-up, respectively;  $t$  test,  $P=0.75$ ,  $n=6$ ). The number of perfused capillaries in the peri-ischemic tissue was reduced compared with baseline at the 3- and 24-hour

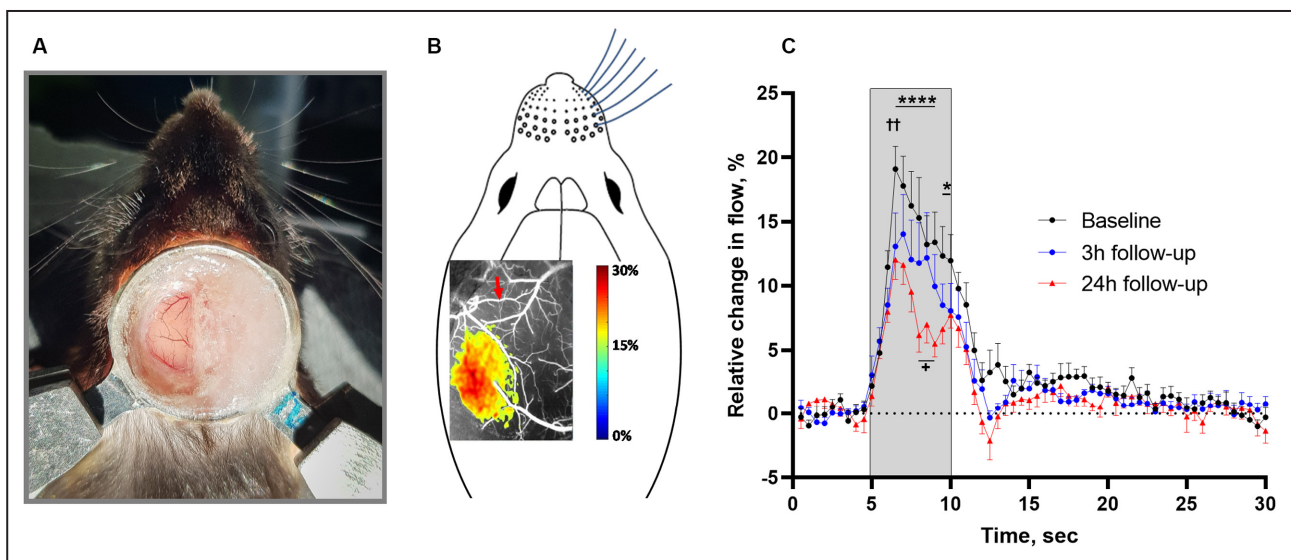


**Figure 3.** Neurovascular coupling responses in the whisker sensory cortex corresponding to the peri-ischemic area were reduced after cerebral ischemia.

**A**, Image of the chronic cranial window preparation and the head fixation of the awake mouse 4 weeks after surgery. **B**, Representative laser speckle contrast image illustrating the local increase in blood flow in the whisker sensory cortex in response to air-puff whisker stimulation at baseline. The red arrow indicates the artery that later was occluded. **C**, The neurovascular coupling response was reduced at the 3- and 24-hour follow-up compared with baseline. The gray area indicates the period when the 5-second whisker stimulation was performed. Error bars=SE. Neurovascular responses were compared using 2-way ANOVA followed by Bonferroni's correction for multiple comparison.  $^{\dagger\dagger}P<0.01$  for 3-hour follow-up vs baseline;  $^*P<0.05$  and  $^{****}P<0.0001$  for 24-hour follow-up vs baseline;  $^+P<0.05$  for 3-hour vs 24-hour follow-up;  $n=6$ .



follow-up (Figure 5E). Furthermore, the incidence of flow stalling, as the % of segments with  $\geq 1$  stall event (Video S2, Figure S1A), and cumulative stalling duration (Figure S1B) were increased at the 3- and 24-hour follow-up compared with baseline. Consequently, the point prevalence of dynamic capillary flow stalling was increased, that is, the share of stalling capillaries of the total number of capillaries at any given time was increased at the 3- and 24-hour follow-up compared with baseline (Figure 5F). The stalling point prevalence remained increased if calculated for the entire field of view instead of being normalized to the total number of perfused capillaries (Figure S1C). The mean duration of each capillary stalling was increased at the 3-hour follow-up but was not statistically different at the 24-hour follow-up compared with baseline (Figure S1D). The mean stalling frequency in capillary segments that exhibited stalling was increased at the 3- and 24-hour follow-up compared with baseline (Figure S1E). The frequency distribution of the mean duration of each capillary stalling is shown in Figure S2. Capillary stalls were not correlated, that is, capillary segments did not stall in a rhythmic nor synchronized manner (Figure S3), although notably, this was with the exception of a single group of spatially related capillaries in 1 mouse that exhibited synchronized rhythmic stalling with a frequency of  $\sim 0.1$  Hz (Video S3, Figure S3). This rhythmic stalling was both observed at baseline and at the 24-hour follow-up.

### Capillary Blood Flow Velocity Increased at the 24-Hour Follow-Up

Blood flow velocity was assessed by phase-resolved Doppler-OCT (Figure 6A through 6C). Blood flow velocity of capillaries in a vertical direction in the peri-ischemic area was assessed in the same region of interest and depth range as the OCT angiograms used for capillary flow stalling analysis. Capillary flow velocity was increased at the 24-hour follow-up compared

with baseline, whereas there was no statistical difference in flow velocity between 3-hour follow-up and baseline (Figure 6D). Mean inner capillary diameter of perfused capillaries was similar at all 3 time points ( $4.67 \pm 0.04 \mu\text{m}$  [baseline; data from 47 capillaries],  $4.53 \pm 0.12 \mu\text{m}$  [3-hour follow-up; data from 28 capillaries], and  $4.69 \pm 0.06 \mu\text{m}$  [24-hour follow-up; data from 37 capillaries],  $n=6$ ).

### Reduced Diameter of Pericyte-Associated Capillaries in the Peri-Ischemic Tissue

Capillary diameter was assessed in perfusion-fixed brain tissue (Figure 7A and 7B, Figure S4A–D). The diameter of capillaries surrounded by pericyte bodies was narrower in the peri-ischemic tissue compared with corresponding pericyte-surrounded capillaries from the contralateral hemisphere (Figure 7C). Diameter of capillaries, where no associated pericyte bodies were observed, was similar in the peri-ischemic and contralateral hemisphere. Capillary density was not different between the 2 hemispheres in the perfusion-fixed brains (Figure 7D).

## DISCUSSION

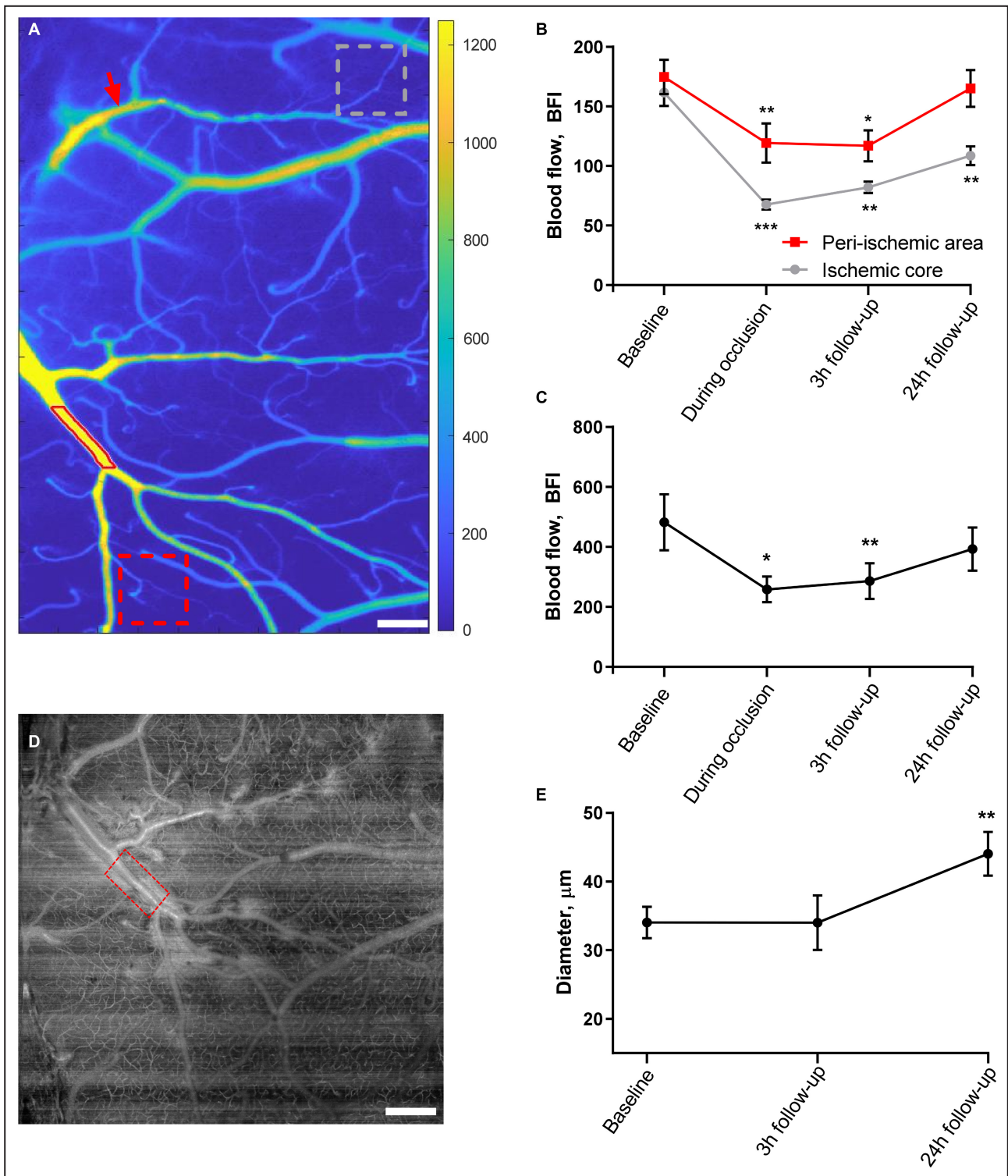
### Capillary Flow Heterogeneity and Its Role in Ischemic Stroke

In this study, neurovascular coupling in the peri-ischemic area was impaired following reperfusion and associated with contraction of peri-ischemic capillary pericytes. Pericyte contraction was associated with a reduced number of perfused capillaries, although the total number of capillaries in the peri-ischemic area was not different from that observed in the contralateral hemisphere and similar to what has previously been reported.<sup>33</sup> The reduced capillary capacity was further worsened by increased dynamic flow stalling in the capillaries that were not permanently occluded. Consistent with reduced

#### Figure 4. Cerebral perfusion was globally reduced 3 hours after ischemia–reperfusion but returned to baseline after 24 hours.

**A**, Tissue perfusion was measured by laser speckle contrast imaging. Regions of interest for tissue perfusion (gray and red dotted boxes in the ischemic core and peri-ischemic area, respectively) and the vessel segmentation (lumen outlined by red line) of the middle cerebral artery (MCA) branch neighboring to the occluded artery are shown. Red arrow indicates the focus point for photothrombosis. Bar= $300 \mu\text{m}$ . **B**, Tissue perfusion was globally reduced 3 hours after ischemia reperfusion in both the ischemic core and the peri-ischemic area (data points for baseline and during occlusion are also shown in Figure 1E). At the 24-hour follow-up, the tissue perfusion of the peri-ischemic area returned to a level similar to the perfusion observed at baseline. **C**, Blood flow in the MCA branch supplying the peri-ischemic area was reduced during the occlusion of the anterior MCA branch and at the 3-hour follow-up but was not statistically different from baseline at the 24-hour follow-up. **D**, Representative optical coherence tomography (OCT) angiogram showing the segment (red box) of the MCA branch neighboring to the occluded artery; same MCA segment as in **A**. Bar= $400 \mu\text{m}$ . **E**, The diameter of the neighboring MCA branch was assessed from this angiogram and revealed vasodilation at the 24-hour follow-up. The MCA diameter was evaluated in absolute values and compared with the baseline using mixed-effects analysis. Error bars=SE. Blood flow (**B** and **C**) was compared with baseline using 1-way ANOVA followed by Dunnett's multiple comparisons tests. Two separate analyses were conducted to evaluate the change in blood flow compared with baseline in the peri-ischemic cortex and the ischemic core (**B**). \* $P < 0.05$ , \*\* $P < 0.01$ , \*\*\* $P < 0.001$ ;  $n=6$ . BFI indicates blood flow index.





capillary capacity, overall parenchymal perfusion was reduced in the peri-ischemic area at the 3-hour follow-up. However, at the 24-hour follow-up, upstream arterial vasodilation was associated with parenchymal perfusion similar to that observed at baseline, although capillary capacity remained suppressed. Consequently, capillary blood flow velocity was increased.

Unequal blood flow distribution in the capillary bed increases capillary transit time heterogeneity associated with impaired oxygen extraction capability.<sup>34</sup> Such undesired blood flow distribution will induce an increasing proportion of erythrocytes passing through the capillary at transit times too short to allow optimal oxygen extraction, also known as “functional shunting.”<sup>11</sup> Cerebral blood flow distribution in patients with

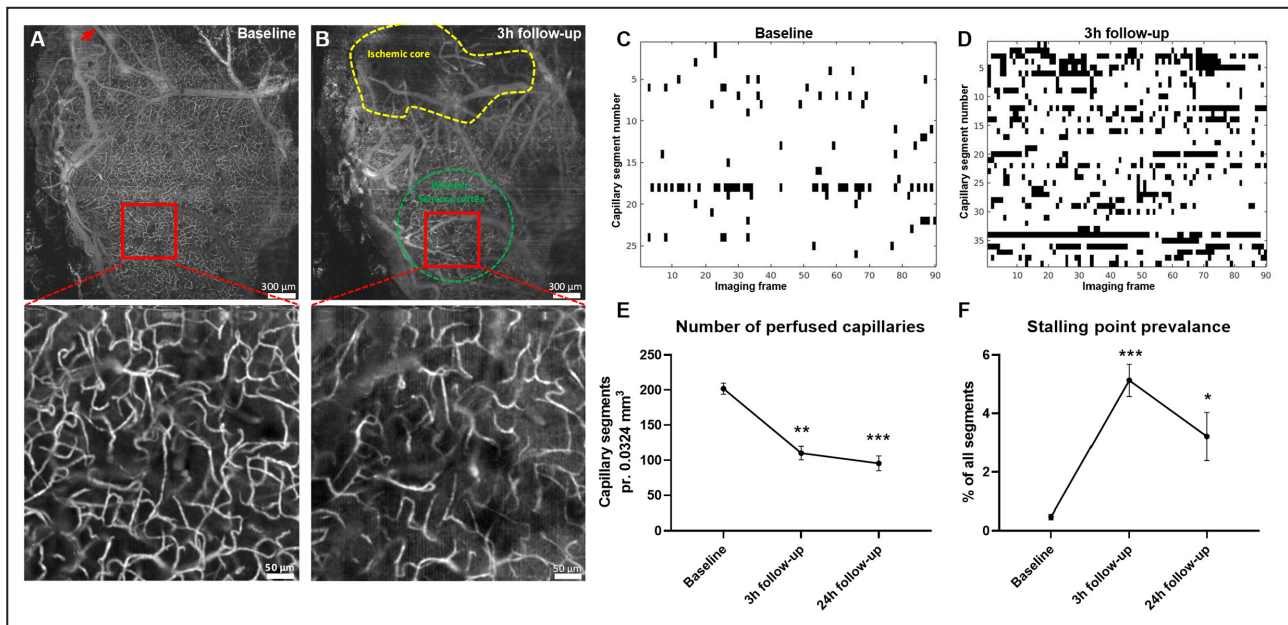


**Figure 5. Reduced number of perfused capillaries and increased dynamic capillary flow stalling after ischemia–reperfusion.** Representative optical coherence tomography (OCT) images of the affected hemisphere at baseline (A) and at the 3-hour follow-up (B). The red arrow indicates the location of photothrombosis (A). Yellow and green dotted areas indicate the ischemic core and the whisker sensory cortex, respectively (B). The high-magnification OCT angiograms were used to assess capillary flow stalling (see Video S2). Representative stallograms from the same mouse at baseline (C) and 3 hours after reperfusion (D) showing the timeline of stalling capillary segments through the 90 consecutive angiograms (stallograms for all mice are shown in Figure S3). E, The number of perfused capillaries was reduced at the 3-hour follow-up and 24-hour follow-up compared with that at baseline. F, The prevalence of dynamic flow stalling was increased at the 3-hour follow-up and 24-hour follow-up compared with that at baseline. Error bars=SE. Data were compared with baseline using repeated measures 1-way ANOVA followed by Dunnett’s multiple comparisons test. \* $P < 0.05$ , \*\* $P < 0.01$ , \*\*\* $P < 0.001$ ;  $n = 6$ .

ischemic stroke assessed by perfusion-weighted magnetic resonance imaging revealed increased capillary transit time heterogeneity in the peri-ischemic regions.<sup>35</sup> Hence, increased capillary transit time heterogeneity may prevent sufficient oxygen delivery to active brain regions mediated through neurovascular coupling in patients with stroke. Accordingly, previous blood oxygenation level dependent functional magnetic resonance imaging studies on patients with stroke reported impaired oxygen extraction in peri-ischemic areas in response to the performance of simple motor tasks.<sup>14,15</sup> Considering data from the present study, disrupted capillary circulation, and thus reduced capillary capacity, may underlie disturbances in neurovascular coupling contributing to futile recanalization in these patients. Neurovascular coupling was further impaired at the 24-hour follow-up compared with the 3-hour follow-up although the stalling point prevalence and number of perfused capillaries were not statistically different at the 2 time points. The upstream artery supplying the sensory cortex was more dilated at the 24-hour follow-up and therefore closer to the maximum dilated state. Hence, reduced capacity for arterial dilation in response to neurovascular activation at the 24-hour follow-up may therefore contribute to impaired

neurovascular coupling. In accordance with this possibility, neurovascular coupling was demonstrated to be compromised in predilated systems.<sup>36</sup>

### Disrupted Capillary Perfusion in Peri-Ischemic Brain Regions

Capillary blockage downstream from the occluded artery has been suggested to explain the no-reflow phenomenon in the ischemic core.<sup>11</sup> There may be several explanations for this outcome, including arterial vasospasm<sup>37</sup> and blood–brain barrier disruption leading to cerebral edema.<sup>38</sup> Another possible explanation is the contraction of capillary pericytes with such activity being potentiated in the brain following ischemia.<sup>6,39–41</sup> Contraction of capillary pericytes under ischemic conditions has also been observed in the kidney and heart.<sup>42–44</sup> This implies that pericyte contraction associated with microvascular failure may be initiated by ischemia after stroke. Another possible explanation is that the pericyte contraction in the peri-ischemic area was elicited by the multiple spreading depolarizations that occurred during arterial occlusion. Experimentally induced spreading depolarization was recently demonstrated to cause contraction of capillary pericytes

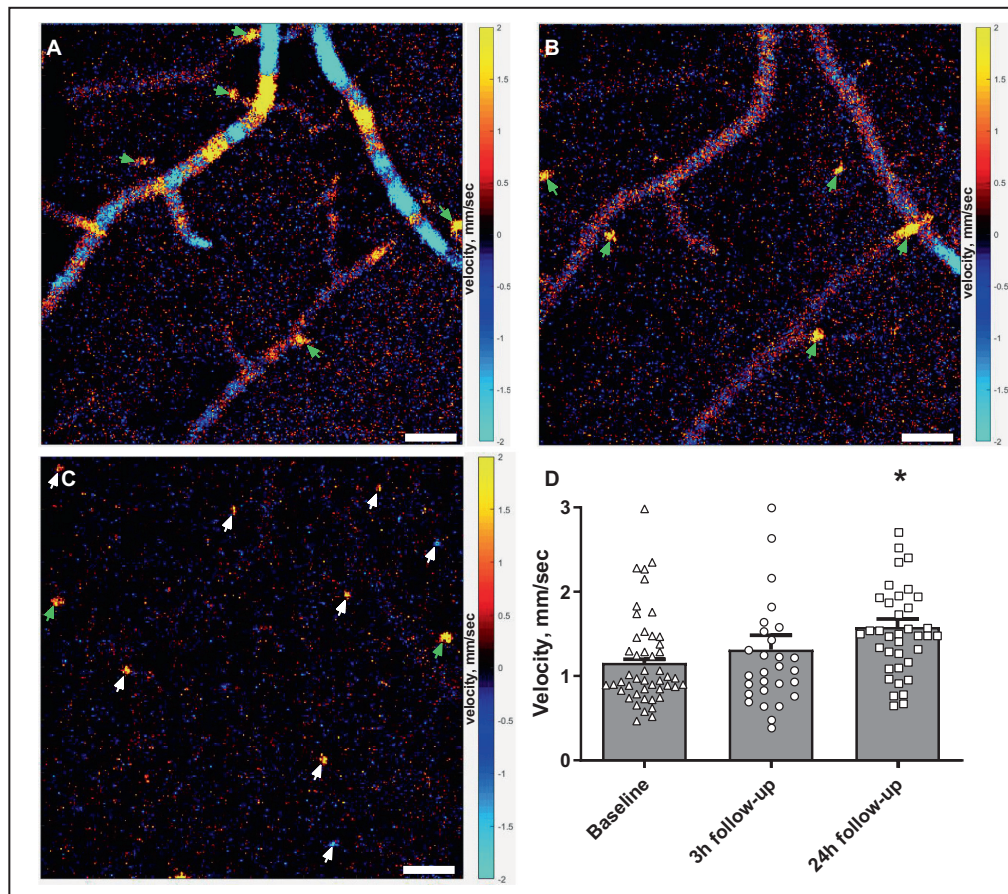


**Figure 6. Capillary flow velocity was increased at the 24-hour follow-up.**

Representative phase-resolved Doppler optical coherence tomography images obtained 33, 53, and 180  $\mu\text{m}$  from the brain surface (A–C, respectively). Pial arteries/veins can be seen on the brain surface, and penetrating arterioles/venules (green arrows) and capillaries (white arrows) are seen in deeper layers of the cortex in a vertical direction. Bars, 50  $\mu\text{m}$  (A–C). Red/yellow and blue/turquoise colors indicate ascending and descending flow, respectively. D, The weighted average capillary flow velocity was similar 3 hours after reperfusion but increased at the 24-hour follow-up compared with that observed at baseline. Error bars=SE. Measurements from capillaries for each mouse at each time point were averaged and plotted as a bar graph. Individual capillary velocity measurements from all mice are plotted on top of bar graphs. The weighted average of capillary flow velocities at the 2 follow-up time points were compared with baseline using repeated measures 1-way ANOVA followed by Dunnett's multiple comparisons test. \* $P < 0.05$   $n = 6$ , measurements from 47, 28, and 37 individual capillaries at baseline, 3-hour, and 24-hour follow-up, respectively.

associated with neurovascular uncoupling in anesthetized mice.<sup>45</sup> In the present study, the first of multiple spreading depolarizations was observed within minutes after the targeted MCA branch was occluded. This caused a significant drop in blood flow in the peri-ischemic area. At the 3-hour follow-up, where a substantially reduced number of perfused capillaries was observed, the perfusion in the peri-ischemic area remained suppressed to a similar level to that observed during the occlusion. This implies that spreading depolarizations during arterial occlusion led to pericyte contraction and thus microvascular failure in the peri-ischemic area. Although spreading depolarizations may cause pericyte constriction in brain tissues,

ischemia has also been shown to induce pericyte constriction in other tissues that cannot exhibit spreading depolarization.<sup>42–44</sup> The specific contributions of reduced oxygen availability and spreading depolarization to pericyte constriction in peri-ischemic brain capillaries after stroke should be further investigated.

In addition to microcirculatory failure, we also observed increased dynamic flow stalling in the peri-ischemic area. Such dynamic stallings were recently reported in penumbra in preclinical animal models of cerebral ischemia.<sup>46,47</sup> Although done in anesthetized mice, the incidence and point prevalence of the capillary stallings are similar to those observed in awake mice in the present study.



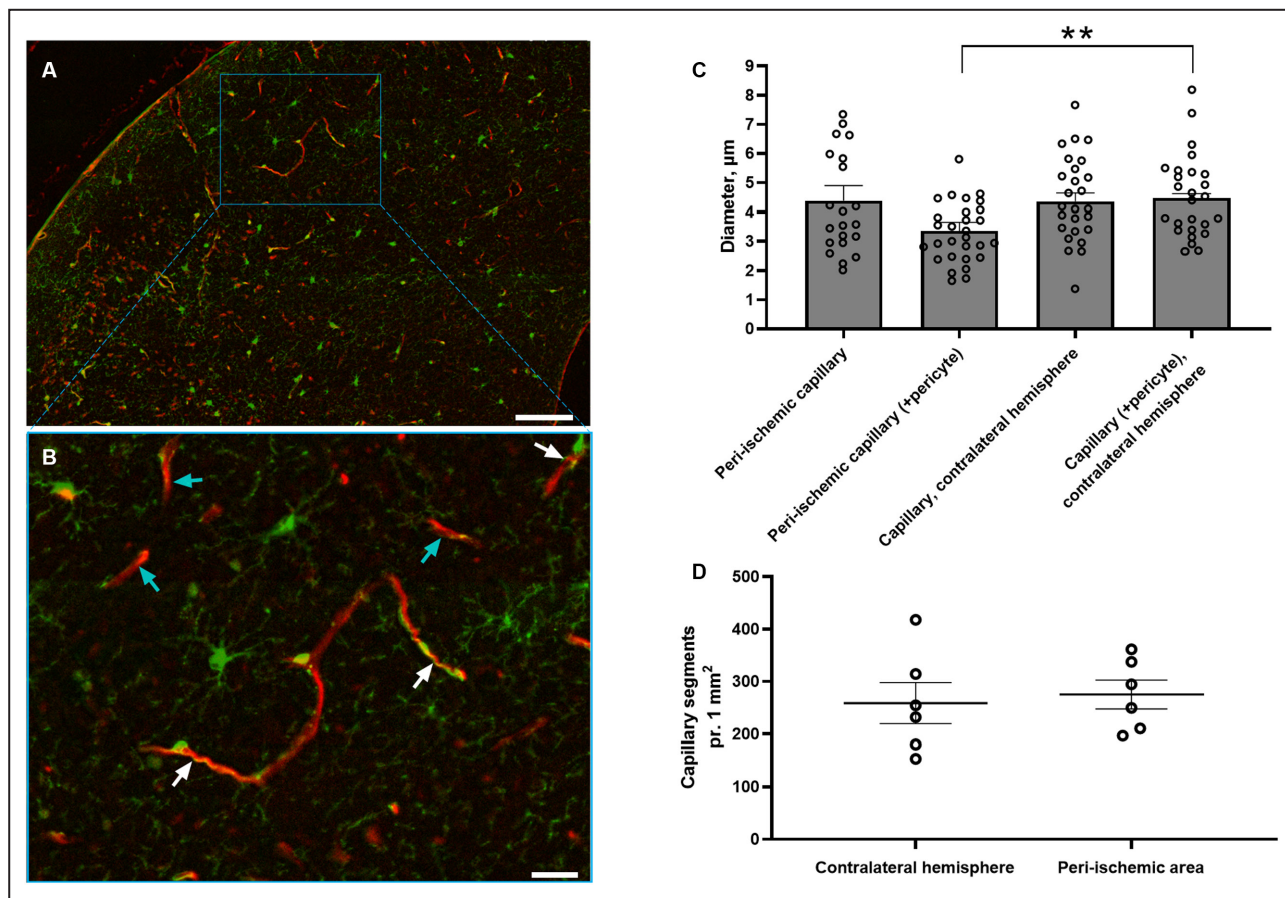


**Figure 7. Diameter of capillary segments surrounded by pericyte bodies was reduced in the peri-ischemic cortex.**

Representative images from the peri-ischemic cortex showing platelet-derived growth factor receptor beta-positive cells in green and lectin in red in low (A) and high magnification (B). White and turquoise arrows indicate capillary segments with and without pericyte bodies, respectively (B). Bars, 100 µm (A) and 25 µm (B). C, Measurements of capillary diameters in each hemisphere for each mouse were averaged and plotted as a bar graph. The diameter of capillaries associated with pericyte bodies in the peri-ischemic cortex was reduced compared with the contralateral cortex. There was no difference in the diameter of capillaries that were not associated with pericyte bodies between the hemispheres. D, The density of capillary segments was similar in both hemispheres. Error bars=SE. Capillary diameter and density in peri-ischemic cortex vs contralateral hemisphere were compared using unpaired *t* test. \*\**P*<0.01, n=6. See splitting of the channels including nucleus staining with 4', 6-diamidino-2-phenylindole in Figure S4.

Some limitations need to be considered in this study. Although an optimized protocol for photothrombosis was used that limits the occlusion to a specific narrow location, it is possible that a few capillaries right below the targeted artery were also occluded. However, surrounding capillaries and larger vessels are not thrombosed when using this protocol.<sup>21</sup> As blood flow was not continuously monitored during the first 3 hours following arterial occlusion, the time to spontaneous reperfusion might vary between subjects and thus affect the outcome. However, all vessels were reperfused within 3 hours. Using a mouse model to study cerebrovascular pathology in ischemic stroke has inherent limitations in reflecting the human state. Thus, it remains to be investigated whether microcirculatory failure in the peri-ischemic area also takes place after ischemic stroke in patients,

although this has been suggested by indirect measurements.<sup>35</sup> Electrical activity in the brain was not measured because mice were carrying a chronic cranial window. Therefore, spreading depolarizations were assessed indirectly based on changes in blood flow. For the same reason, we cannot exclude the possibility that neuronal dysfunction after spreading depolarization may also contribute to impaired neurovascular coupling. Locomotion of the awake mouse was not corrected for, which may affect neurovascular coupling in the sensory cortex.<sup>48,49</sup> Further, potential hypoxia during the perfusion-fixation procedure may affect the morphology and contractile state of pericytes, although the unchanged contractile state of pericytes from the contralateral hemisphere suggested that this was not the case. Finally, only the hemisphere where the arterial occlusion took place



was examined *in vivo*. Whether disruption of the microcirculation and thus impaired neurovascular coupling is also affecting the contralateral hemisphere remains to be investigated.

### Conclusions

Findings from the present study contribute to an improved understanding of the cerebrovascular changes outside the ischemic core that may contribute to futile recanalization. Key insights into the vascular events during and after cerebral ischemia are provided, and a novel link between these microcirculatory changes and dysfunctional neurovascular coupling after stroke is proposed. These findings call for future studies on how to enhance overall passage of blood cells through the capillary circulation and thus restore coupling between the neuronal tissue and the vasculature in patients with ischemic stroke.

### ARTICLE INFORMATION

Received January 19, 2023; accepted April 19, 2023.

#### Affiliations

Department of Biomedicine, Aarhus University, Aarhus, Denmark (C.S., H.Ø.G., V.V.M.); Neurophotonics Center, Department of Biomedical Engineering, Boston University, Boston, MA (C.S., J.T.G., J.T., D.A.B.); Center of Functionally Integrative Neuroscience, Institute for Clinical Medicine, Aarhus University, Aarhus, Denmark (E.G.-J.); Department of Biomedical Engineering, Southern University of Science and Technology, Shenzhen, China (J.T.); Biomedical Science, School of Health, University of the Sunshine Coast, Sippy Downs, Australia (S.L.S.); and Centre for Clinical Research, Faculty of Medicine, The University of Queensland, Brisbane, Australia (S.L.S.).

#### Acknowledgments

We would like to thank Dr Dmitry Postnov and Prof Andrew Dunn for software to acquire and analyze laser speckle data. We also thank John Jiang, Jane Holbæk Rønn, and Anna Bay Nielsen for excellent technical assistance. Finally, we thank Prof Leif Østergaard and Prof Christian Aalkjaer for fruitful scientific discussions. Author contributions: Christian Staehr, Shaun L. Sandow, David A. Boas, and Vladimir V. Matchkov contributed to the conception and design of the study. Christian Staehr carried out the experiments. Christian Staehr, John T. Giblin, Eugenio Gutiérrez-Jiménez, and Jianbo Tang analyzed and interpreted the data. Christian Staehr and Vladimir V. Matchkov prepared the draft and finalized the article. All authors provided critical feedback and approved the final version of the article.

#### Sources of Funding

This work was supported by The International Network Programme by the Danish Agency for Science and Higher Education (nr.: 8073-00007B), The Independent Research Fund Denmark—Medical Sciences (8020-00084B), Lundbeck Foundation (R344-2020-952), and Helga & Peter Korning's Foundation (#2021-35).

#### Disclosures

None.

#### Supplemental Material

Data S1.  
Tables S1–S2.  
Figures S1–S4.  
Video S1.  
Video S2.  
Videos S3.

### REFERENCES

- Nippert AR, Biesecker KR, Newman EA. Mechanisms mediating functional hyperemia in the brain. *Neuroscientist*. 2018;24:73–83. doi: 10.1177/1073858417703033
- Longden TA, Dabertrand F, Koide M, Gonzales AL, Tykocki NR, Brayden JE, Hill-Eubanks D, Nelson MT. Capillary K<sup>+</sup>-sensing initiates retrograde hyperpolarization to increase local cerebral blood flow. *Nature Neuroscience*. 2017;20:717–726. doi: 10.1038/nn.4533
- Staehr C, Rajanathan R, Postnov DD, Hangaard L, Bouzinaova EV, Lykke-Hartmann K, Bach FW, Sandow SL, Aalkjaer C, Matchkov VV. Abnormal neurovascular coupling as a cause of excess cerebral vasodilation in familial migraine. *Cardiovasc Res*. 2020;116:2009–2020. doi: 10.1093/cvr/cvz306
- Erdener ŞE, Küreli G, Dalkara T. Contractile apparatus in CNS capillary pericytes. *Neurophotonics*. 2022;9:021904. doi: 10.1117/1.NPh.9.2.021904
- Bandopadhyay R, Orte C, Lawrenson JG, Reid AR, De Silva S, Allt G. Contractile proteins in pericytes at the blood-brain and blood-retinal barriers. *J Neurocytol*. 2001;30:35–44. doi: 10.1023/a:1011965307612
- Hall CN, Reynell C, Gesslein B, Hamilton NB, Mishra A, Sutherland BA, O'Farrell FM, Buchan AM, Lauritzen M, Attwell D. Capillary pericytes regulate cerebral blood flow in health and disease. *Nature*. 2014;508:55–60. doi: 10.1038/nature13165
- Gonzales AL, Klug NR, Moshkforoush A, Lee JC, Lee FK, Shui B, Tsoukias NM, Kotlikoff MI, Hill-Eubanks D, Nelson MT. Contractile pericytes determine the direction of blood flow at capillary junctions. *Proc Natl Acad Sci USA*. 2020;117:27022–27033. doi: 10.1073/pnas.1922755117
- Hill RA, Tong L, Yuan P, Murkinati S, Gupta S, Grutzendler J. Regional blood flow in the normal and ischemic brain is controlled by arteriolar smooth muscle cell contractility and not by capillary pericytes. *Neuron*. 2015;87:95–110. doi: 10.1016/j.neuron.2015.06.001
- Kisler K, Nelson AR, Rege SV, Ramanathan A, Wang Y, Ahuja A, Lazic D, Tsai PS, Zhao Z, Zhou Y, et al. Pericyte degeneration leads to neurovascular uncoupling and limits oxygen supply to brain. *Nat Neurosci*. 2017;20:406–416. doi: 10.1038/nn.4489
- Fernández-Klett F, Offenhauser N, Dirnagl U, Priller J, Lindauer U. Pericytes in capillaries are contractile *in vivo*, but arterioles mediate functional hyperemia in the mouse brain. *Proc Natl Acad Sci USA*. 2010;107:22290–22295. doi: 10.1073/pnas.1011321108
- Østergaard L, Jespersen SN, Mouridsen K, Mikkelsen IK, Jonsdottir K, Tietze A, Blicher JU, Aamand R, Hjort N, Iversen NK, et al. The role of the cerebral capillaries in acute ischemic stroke: the extended penumbra model. *J Cereb Blood Flow Metab*. 2013;33:635–648. doi: 10.1038/jcbfm.2013.18
- Shi ZS, Liebeskind DS, Xiang B, Ge SG, Feng L, Albers GW, Budzik R, Devlin T, Gupta R, Jansen O, et al. Predictors of functional dependence despite successful revascularization in large-vessel occlusion strokes. *Stroke*. 2014;45:1977–1984. doi: 10.1161/strokeaha.114.005603
- Molina CA. Futile recanalization in mechanical embolectomy trials: a call to improve selection of patients for revascularization. *Stroke*. 2010;41:842–843. doi: 10.1161/strokeaha.110.580266
- Pineiro R, Pendlebury S, Johansen-Berg H, Matthews PM. Altered hemodynamic responses in patients after subcortical stroke measured by functional MRI. *Stroke*. 2002;33:103–109. doi: 10.1161/hs0102.100482
- Krainik A, Hund-Georgiadis M, Zysset S, von Cramon DY. Regional impairment of cerebrovascular reactivity and BOLD signal in adults after stroke. *Stroke*. 2005;36:1146–1152. doi: 10.1161/01.STR.0000166178.40973.a7
- Lin WH, Hao Q, Rosengarten B, Leung WH, Wong KS. Impaired neurovascular coupling in ischaemic stroke patients with large or small vessel disease. *Eur J Neurol*. 2011;18:731–736. doi: 10.1111/j.1468-1331.2010.03262.x
- D'Esposito M, Deouell LY, Gazzaley A. Alterations in the BOLD fMRI signal with ageing and disease: a challenge for neuroimaging. *Nat Rev Neurosci*. 2003;4:863–872. doi: 10.1038/nrn1246
- Kelly DM, Jones TH. Testosterone: a vascular hormone in health and disease. *J Endocrinol*. 2013;217:R47–R71. doi: 10.1530/joe-12-0582
- Cid MC, Kleinman HK, Grant DS, Schnaper HW, Fauci AS, Hoffman GS. Estradiol enhances leukocyte binding to tumor necrosis factor (TNF)-stimulated endothelial cells via an increase in TNF-induced adhesion molecules E-selectin, intercellular adhesion molecule type 1, and

- vascular cell adhesion molecule type 1. *J Clin Invest*. 1994;93:17–25. doi: 10.1172/jci116941
20. Zhao L, Mulligan MK, Nowak TS Jr. Substrain- and sex-dependent differences in stroke vulnerability in C57BL/6 mice. *J Cereb Blood Flow Metab*. 2019;39:426–438. doi: 10.1177/0271678x17746174
  21. Sunil S, Erdener SE, Lee BS, Postnov D, Tang J, Kura S, Cheng X, Chen IA, Boas DA, Kiliç K. Awake chronic mouse model of targeted pial vessel occlusion via photothrombosis. *Neurophotonics*. 2020;7:015005. doi: 10.1117/1.NPh.7.1.015005
  22. Sigler A, Goroshkov A, Murphy TH. Hardware and methodology for targeting single brain arterioles for photothrombotic stroke on an upright microscope. *J Neurosci Methods*. 2008;170:35–44. doi: 10.1016/j.jneumeth.2007.12.015
  23. Erdener ŞE, Tang J, Sajjadi A, Kiliç K, Kura S, Schaffer CB, Boas DA. Spatio-temporal dynamics of cerebral capillary segments with stalling red blood cells. *J Cereb Blood Flow Metab*. 2019;39:886–900. doi: 10.1177/0271678x17743877
  24. Srinivasan VJ, Jiang JY, Yaseen MA, Radhakrishnan H, Wu W, Barry S, Cable AE, Boas DA. Rapid volumetric angiography of cortical microvasculature with optical coherence tomography. *Opt Lett*. 2010;35:43–45. doi: 10.1364/ol.35.000043
  25. Tang J, Erdener SE, Fu B, Boas DA. Capillary red blood cell velocimetry by phase-resolved optical coherence tomography. *Opt Lett*. 2017;42:3976–3979. doi: 10.1364/ol.42.003976
  26. Tang J, Erdener SE, Sunil S, Boas DA. Normalized field autocorrelation function-based optical coherence tomography three-dimensional angiography. *J Biomed Opt*. 2019;24:1–8. doi: 10.1117/1.Jbo.24.3.036005
  27. Boas D, Dunn A. Laser speckle contrast imaging in biomedical optics. *J Biomed Opt*. 2010;15:011109. doi: 10.1117/1.3285504
  28. Kirkpatrick SJ, Duncan DD, Wells-Gray EM. Detrimental effects of speckle-pixel size matching in laser speckle contrast imaging. *Opt Lett*. 2008;33:2886–2888. doi: 10.1364/ol.33.002886
  29. Postnov DD, Cheng X, Erdener SE, Boas DA. Choosing a laser for laser speckle contrast imaging. *Sci Rep*. 2019;9:2542. doi: 10.1038/s41598-019-39137-x
  30. Postnov DD, Tuchin VV, Sosnovtseva O. Estimation of vessel diameter and blood flow dynamics from laser speckle images. *Biomed Opt Express*. 2016;7:2759–2768. doi: 10.1364/boe.7.002759
  31. Staehr C, Hangaard L, Bouzinova EV, Kim S, Rajanathan R, Boegh Jessen P, Luque N, Xie Z, Lykke-Hartmann K, Sandow SL, et al. Smooth muscle Ca(2+) sensitization causes hypercontractility of middle cerebral arteries in mice bearing the familial hemiplegic migraine type 2 associated mutation. *J Cereb Blood Flow Metab*. 2019;39:1570–1587. doi: 10.1177/0271678x18761712
  32. McDowell KP, Berthiaume AA, Tieu T, Hartmann DA, Shih AY. VasoMetrics: unbiased spatiotemporal analysis of microvascular diameter in multi-photon imaging applications. *Quant Imaging Med Surg*. 2021;11:969–982. doi: 10.21037/qjms-20-920
  33. Rolfes L, Riek-Burchardt M, Pawlitzki M, Minnerup J, Bock S, Schmidt M, Meuth SG, Gunzer M, Neumann J. Neutrophil granulocytes promote flow stagnation due to dynamic capillary stalls following experimental stroke. *Brain Behav Immun*. 2021;93:322–330. doi: 10.1016/j.bbi.2021.01.011
  34. Jespersen SN, Østergaard L. The roles of cerebral blood flow, capillary transit time heterogeneity, and oxygen tension in brain oxygenation and metabolism. *J Cereb Blood Flow Metab*. 2012;32:264–277. doi: 10.1038/jcbfm.2011.153
  35. Engedal TS, Hjort N, Hougaard KD, Simonsen CZ, Andersen G, Mikkelsen IK, Boldsen JK, Eskildsen SF, Hansen MB, Angleys H, et al. Transit time homogenization in ischemic stroke – a novel biomarker of penumbral microvascular failure? *J Cereb Blood Flow Metab*. 2018;38:2006–2020. doi: 10.1177/0271678x17721666
  36. Sicard KM, Duong TQ. Effects of hypoxia, hyperoxia, and hypercapnia on baseline and stimulus-evoked BOLD, CBF, and CMRO2 in spontaneously breathing animals. *NeuroImage*. 2005;25:850–858. doi: 10.1016/j.neuroimage.2004.12.010
  37. Guldbrandsen HO, Staehr C, Iversen NK, Postnov DD, Matchkov VV. Does Src kinase mediated vasoconstriction impair penumbral reperfusion? *Stroke*. 2021;52:e250–e258. doi: 10.1161/strokeaha.120.032737
  38. Ng FC, Churilov L, Yassi N, Kleinig TJ, Thijs V, Wu TY, Shah DG, Dewey HM, Sharma G, Desmond PM, et al. Microvascular dysfunction in blood-brain barrier disruption and hypoperfusion within the infarct posttreatment are associated with cerebral edema. *Stroke*. 2021;53:Strokeaha121036104. doi: 10.1161/strokeaha.121.036104
  39. Yemisci M, Gursoy-Ozdemir Y, Vural A, Can A, Topalkara K, Dalkara T. Pericyte contraction induced by oxidative-nitrative stress impairs capillary reflow despite successful opening of an occluded cerebral artery. *Nat Med*. 2009;15:1031–1037. doi: 10.1038/nm.2022
  40. Dalkara T. Pericytes. *Stroke*. 2019;50:2985–2991. doi: 10.1161/STROKEAHA.118.023590
  41. Korte N, Ilkan Z, Pearson CL, Pfeiffer T, Singhal P, Rock JR, Sethi H, Gill D, Attwell D, Tammaro P. The Ca2+-gated channel TMEM16A amplifies capillary pericyte contraction and reduces cerebral blood flow after ischemia. *J Clin Invest*. 2022;132:132. doi: 10.1172/jci154118
  42. O'Farrell FM, Mastitskaya S, Hammond-Haley M, Freitas F, Wah WR, Attwell D. Capillary pericytes mediate coronary no-reflow after myocardial ischaemia. *eLife*. 2017;6:e29280. doi: 10.7554/eLife.29280
  43. Freitas F, Attwell D. Pericyte-mediated constriction of renal capillaries evokes no-reflow and kidney injury following ischaemia. *eLife*. 2022;11:e74211. doi: 10.7554/eLife.74211
  44. Le DE, Zhao Y, Kaul S. Persistent coronary vasomotor tone during myocardial ischemia occurs at the capillary level and may involve pericytes. *Front Cardiovasc Med*. 2022;9:9. doi: 10.3389/fcvm.2022.930492
  45. Khenouf L, Gesslein B, Brazhe A, Octeau JC, Kutuzov N, Khakh BS, Lauritzen M. Active role of capillary pericytes during stimulation-induced activity and spreading depolarization. *Brain*. 2018;141:2032–2046. doi: 10.1093/brain/awy143
  46. Erdener ŞE, Tang J, Kiliç K, Postnov D, Giblin JT, Kura S, Chen IA, Vayisoğlu T, Sakadžić S, Schaffer CB, et al. Dynamic capillary stalls in reperfused ischemic penumbra contribute to injury: a hyperacute role for neutrophils in persistent traffic jams. *J Cereb Blood Flow Metab*. 2021;41:236–252. doi: 10.1177/0271678x20914179
  47. El Amki M, Glüeck C, Binder N, Middleham W, Wyss MT, Weiss T, Meister H, Luft A, Weller M, Weber B, et al. Neutrophils obstructing brain capillaries are a major cause of no-reflow in ischemic stroke. *Cell Rep*. 2020;33:108260. doi: 10.1016/j.celrep.2020.108260
  48. Eyre B, Shaw K, Sharp P, Boorman L, Lee L, Shabir O, Berwick J, Howarth C. The effects of locomotion on sensory-evoked haemodynamic responses in the cortex of awake mice. *Scientific Reports*. 2022;12:6236. doi: 10.1038/s41598-022-10195-y
  49. Zhang Q, Turner KL, Gheres KW, Hossain MS, Drew PJ. Behavioral and physiological monitoring for awake neurovascular coupling experiments: a how-to guide. *Neurophotonics*. 2022;9:021905. doi: 10.1117/1.NPh.9.2.021905

# **SUPPLEMENTAL MATERIAL**

**Table S1. Baseline characteristics of mice.**

		Lower 95% CI	Upper 95% CI
Number of mice ( <i>n</i> )	6	-	-
Age (weeks)	24-26	-	-
Sex	Females	-	-
Mouse strain	C57BL/6	-	-
Avg. 2 <sup>nd</sup> MCA branch diameter ( $\mu\text{m}$ )	34.02	28.16	39.87
Avg. 2 <sup>nd</sup> MCA branch blood flow (BFI)	482	242	722
Density of perfused capillaries (pr. 0.0324 mm <sup>3</sup> )	202	182	222

The diameter and blood flow index (BFI) of the middle cerebral artery (MCA) were assessed using optical coherence tomography and laser speckle contrast imaging, respectively. CI, confidence interval.

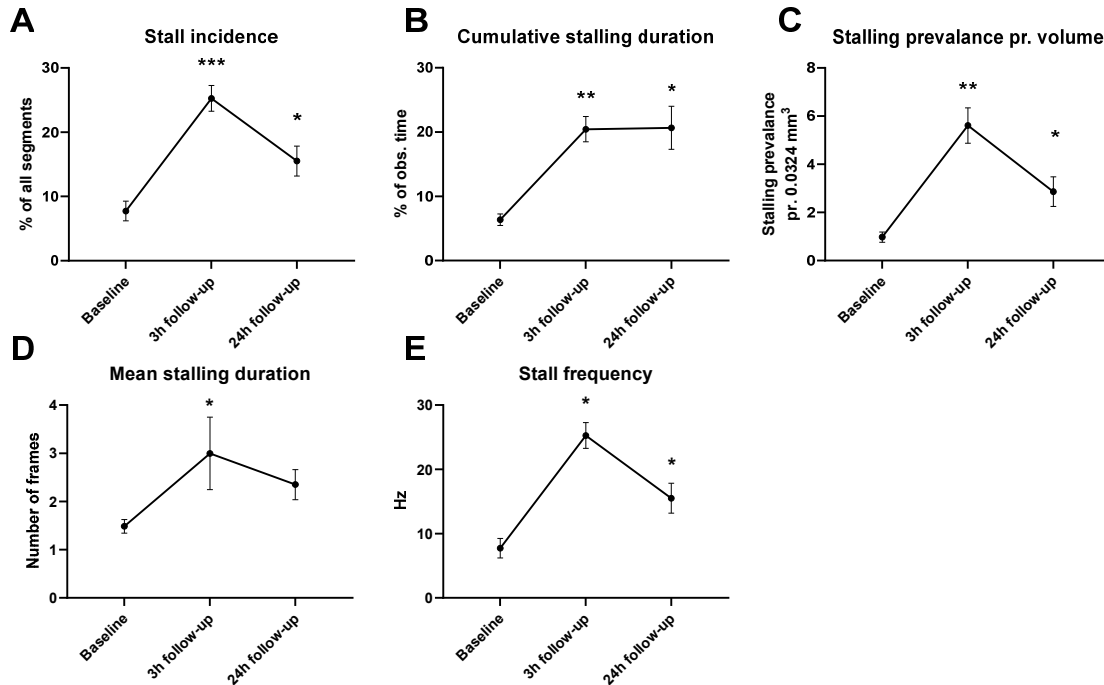


**Table S2. Properties of spreading depolarizations during arterial occlusion.**

	Mean $\pm$ SEM	Lower 95% CI	Upper 95% CI
Spreading depolarization propagation velocity (mm/min)	4.16 $\pm$ 0.21	3.61	4.71
Time from beginning of occlusion to first spreading depolarization (sec)	143.30 $\pm$ 32.01	61.06	225.6
Initial spreading depolarization hypoperfusion duration (sec)	36.25 $\pm$ 1.25	32.27	40.23
Amplitude of initial spreading depolarization hypoperfusion (%)	-33.60 $\pm$ 6.01	-52.71	-14.48
Spreading depolarization hyperperfusion duration (sec)	96.38 $\pm$ 6.67	79.24	113.50
Amplitude of spreading depolarization hyperperfusion (%)	72.49 $\pm$ 10.59	45.28	99.70
Number of spreading depolarizations during 60 min occlusion	11.33 $\pm$ 1.86	6.56	16.10

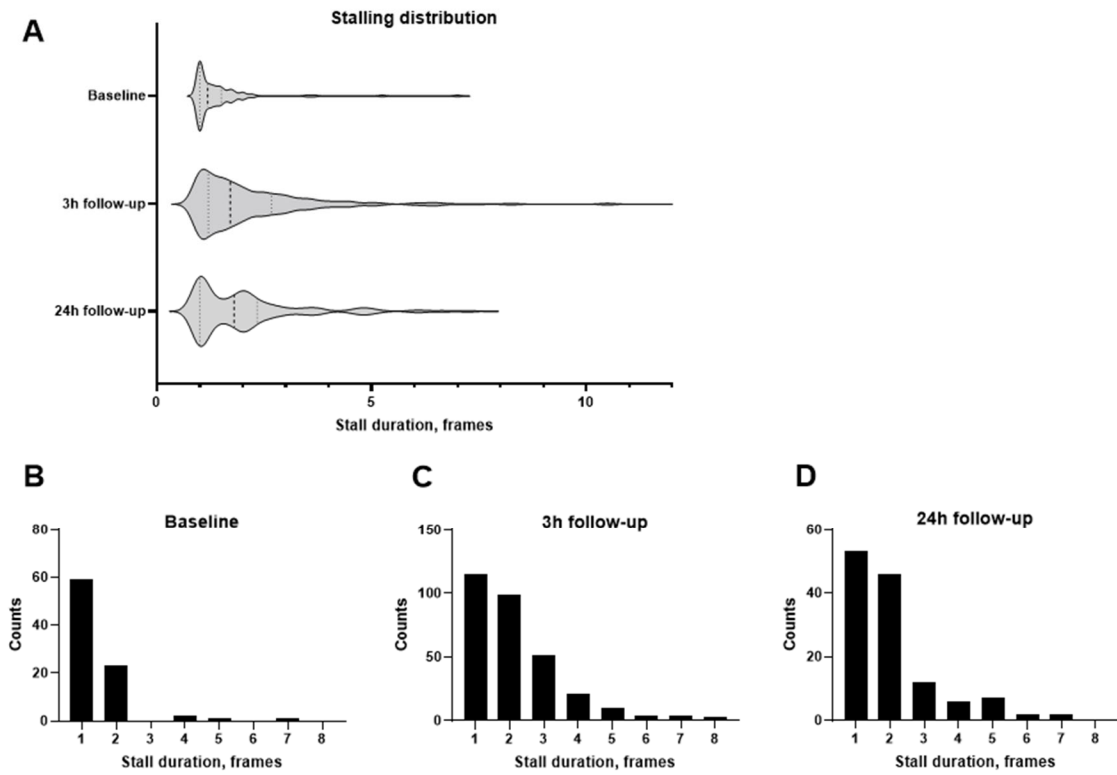
The first spreading depolarization in each mouse led to initial hypoperfusion followed by a wave of hyperperfusion and subsequently sustained hypoperfusion. The subsequent spreading depolarizations during the sustained hypoperfusion were associated with a wave of hyperperfusion. Peak amplitude was calculated as the maximal change in blood flow during spreading depolarization compared to an average of flow 1 min preceding the spreading depolarization. See Fig. 2 for representative traces and Video S1. CI, confidence interval.  $n=6$ .

**Figure S1. Dynamic capillary flow stalling was increased after reperfusion.**



**A**, The incidence of capillary flow stalling was increased at the 3 and 24h follow-up compared with baseline. **B**, Cumulative stalling duration was increased at the 3 and 24h follow-up compared with baseline. **C**, Stalling prevalence normalized to the field of view, i.e., 600x600x90  $\mu\text{m}$ , was increased at the 3 and 24h follow-up compared with baseline (point prevalence normalized to the number of perfused capillaries is shown in Fig. 5F). **D**, The mean stalling duration was increased at the 3h follow-up, but not statistically different 24h after reperfusion compared with baseline. **E**, The mean stalling frequency of capillary segments that exhibited stalling was increased at the 3 and 24h follow-up compared with baseline. Error bars as standard error. Data were compared with baseline using repeated measures 1-way ANOVA followed by Dunnett's multiple comparisons test. \*, \*\*, \*\*\*  $P < 0.05, 0.01, 0.001$ ;  $n = 6$ .

**Figure S2. Frequency distribution of mean duration of each capillary stalling.**



**A**, Distribution of stalling durations for all capillary stallings as a violin plot. Histograms show the frequency distribution of stalling durations at baseline (**B**), 3h (**C**) and 24h follow-up (**D**). Optical coherence tomography framerate=0.167 Hz.  $n=6$ .

**Figure S3. Point prevalence, stallogram, and Pearson correlation plot for each mouse.**

*Left panel:* Traces of point prevalence of capillary flow stalling (y-axis) is shown for each frame (x-axis) and suggests that capillary stalls are not rhythmic at baseline nor after reperfusion.

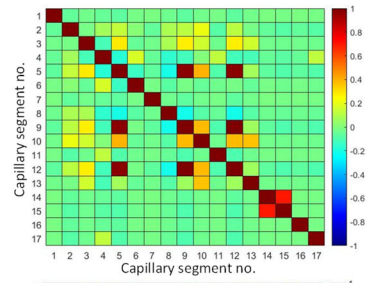
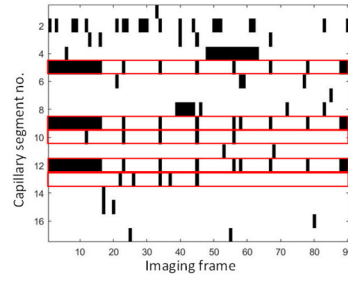
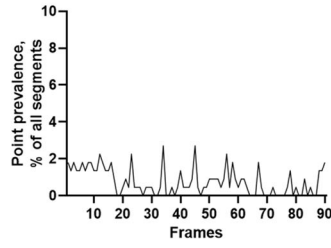
*Middle panel:* Stallograms in the middle panel showing the timeline of stalling capillary segments through the 90 consecutive angiograms where black indicates capillary stalling.

*Right panel:* Pearson correlation analysis of capillary stalls suggested that capillary stalling is not synchronized. One exception was a group of spatially related capillaries in mouse #1 that exhibited synchronized and rhythmic stalling, which is indicated with red rectangles in the stallograms. The rhythmic stalls are also shown in Video S3.

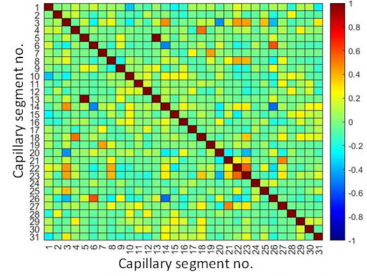
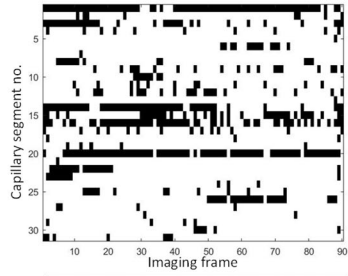
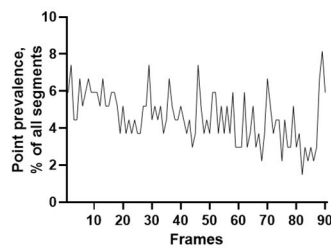
Figure S3

Mouse #1

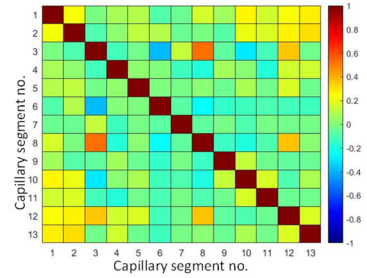
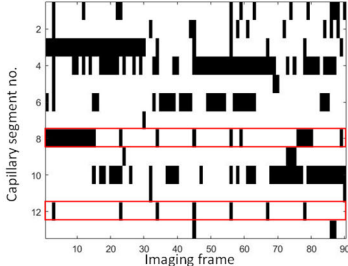
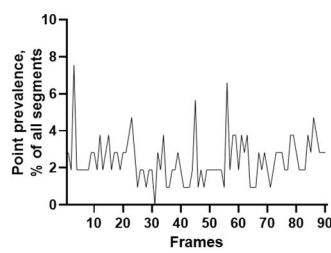
Baseline



3h follow-up

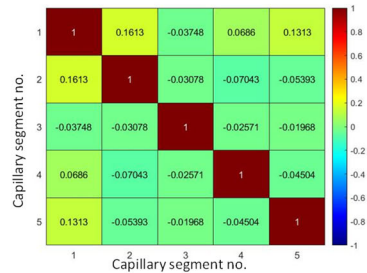
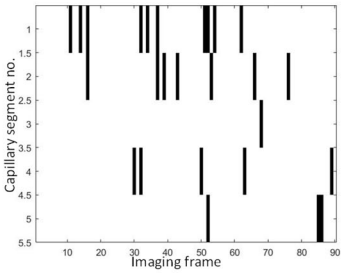
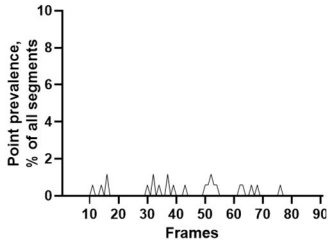


24h follow-up

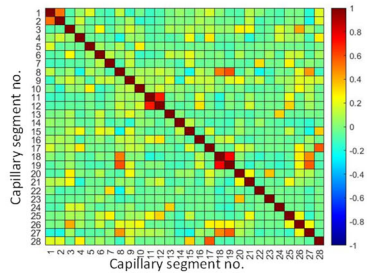
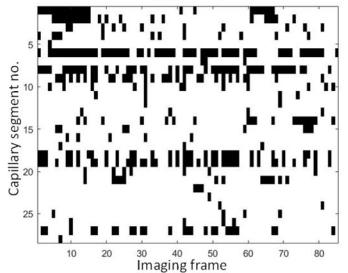
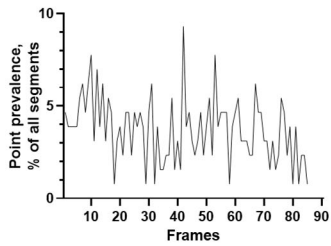


Mouse #2

Baseline



3h follow-up



24h follow-up

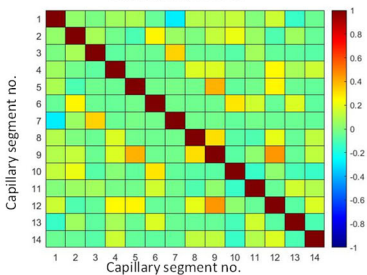
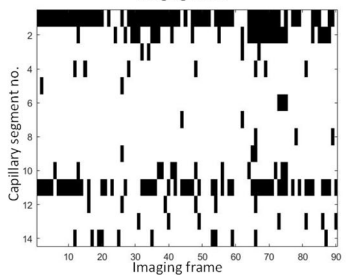
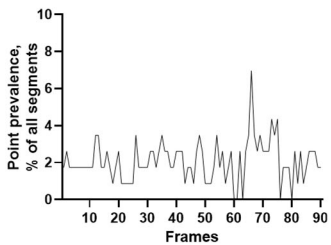
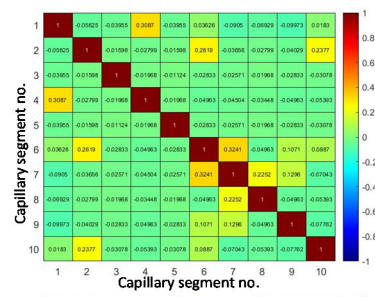
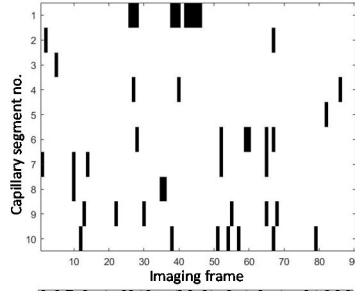
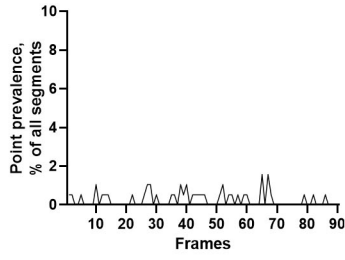




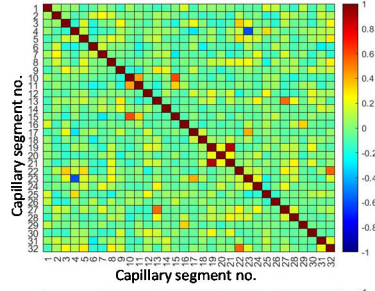
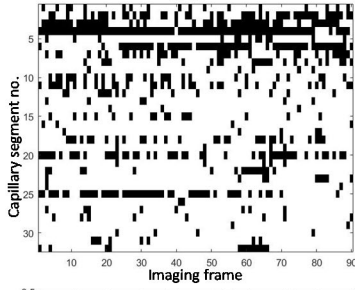
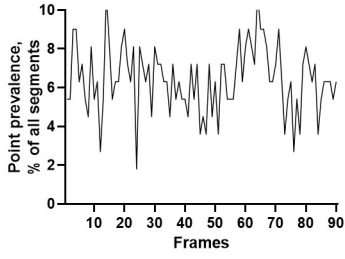
Figure S3, continued

**Mouse #3**

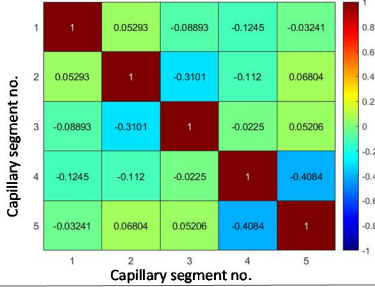
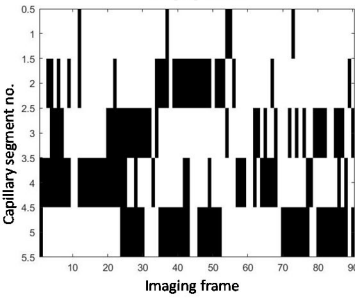
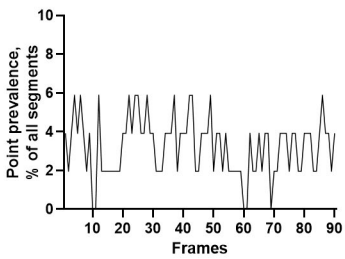
Baseline



3h follow-up

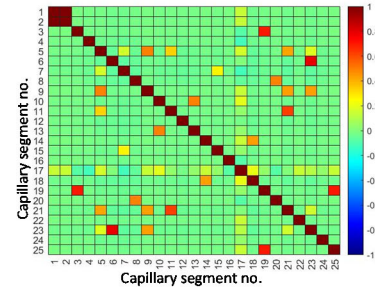
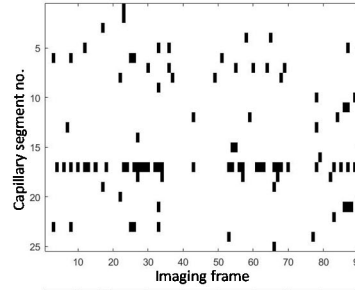
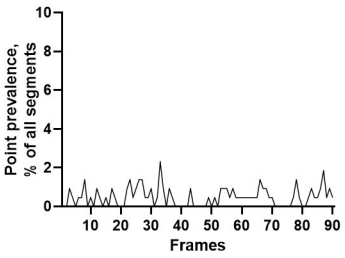


24h follow-up

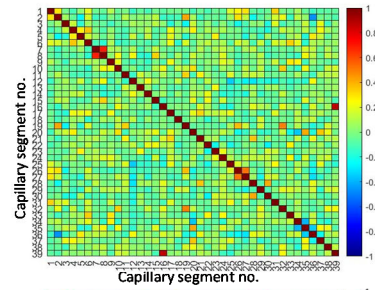
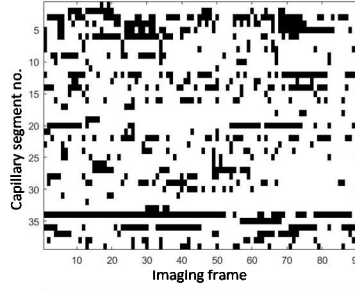
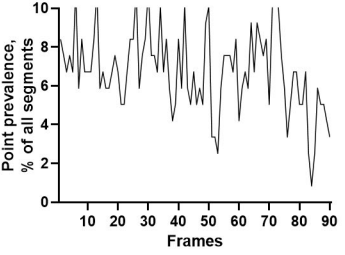


**Mouse #4**

Baseline



3h follow-up



24h follow-up

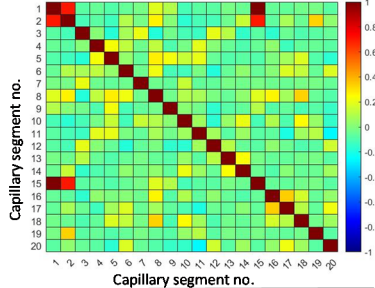
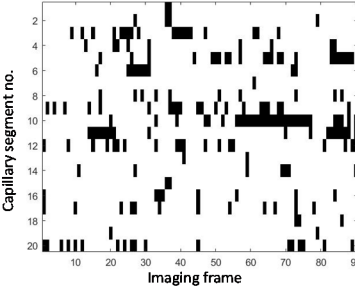
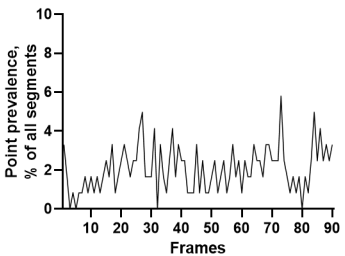
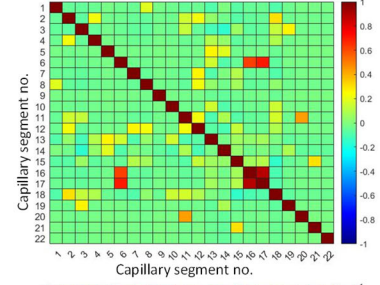
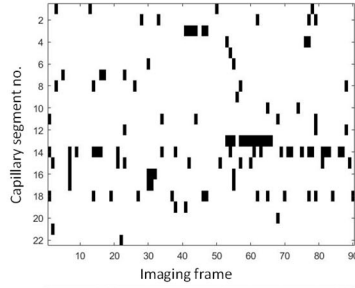
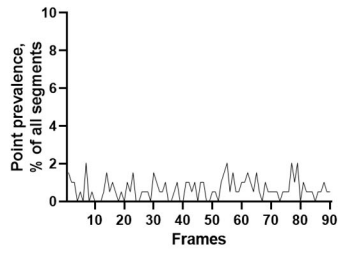


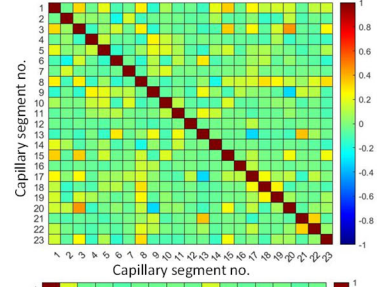
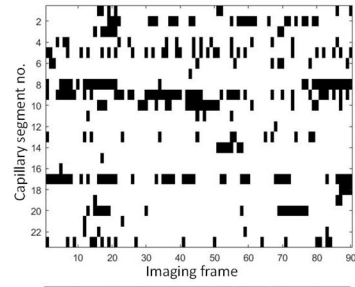
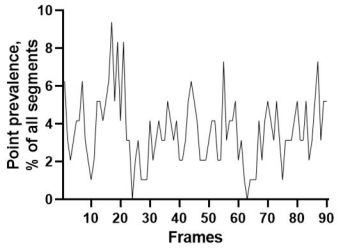
Figure S3, continued

**Mouse #5**

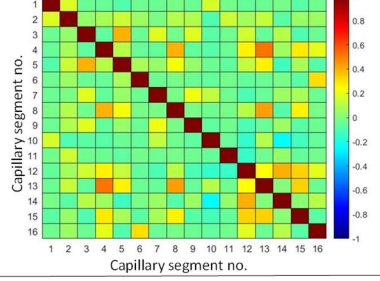
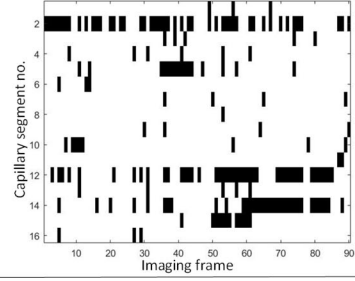
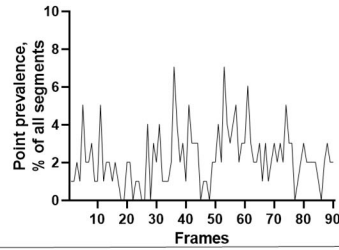
Baseline



3h follow-up

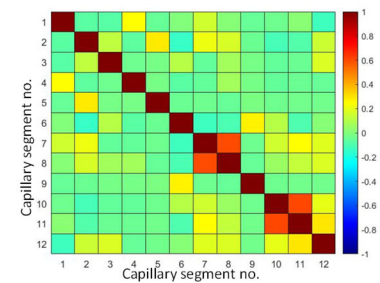
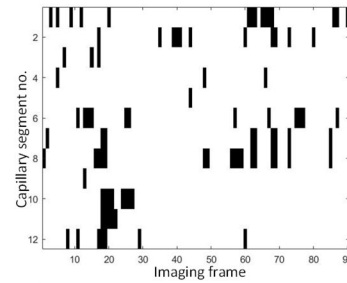
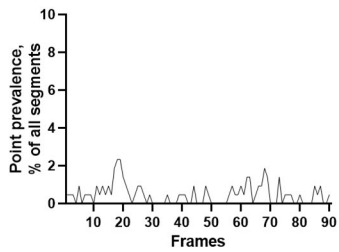


24h follow-up

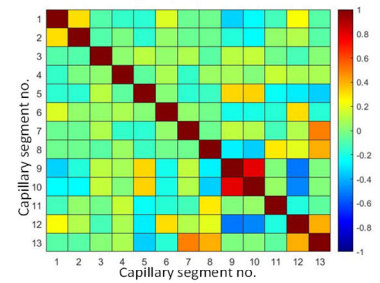
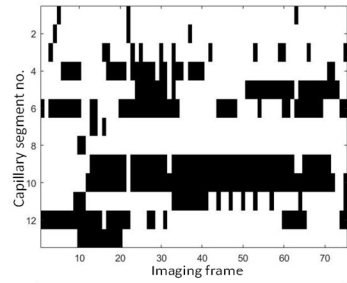
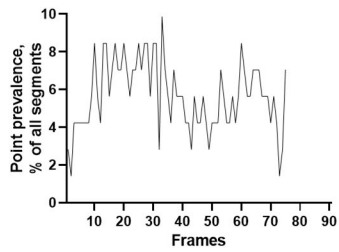


**Mouse #6**

Baseline



3h follow-up



24h follow-up

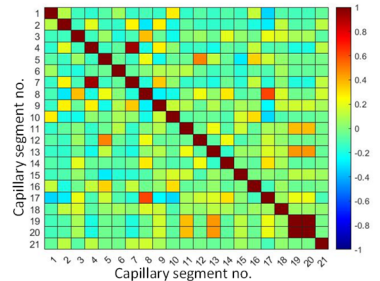
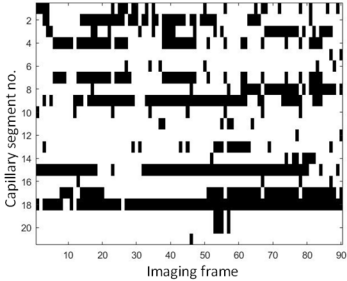
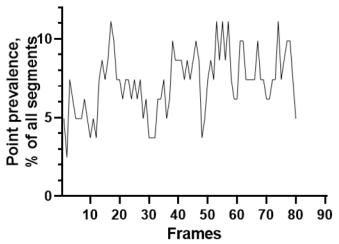
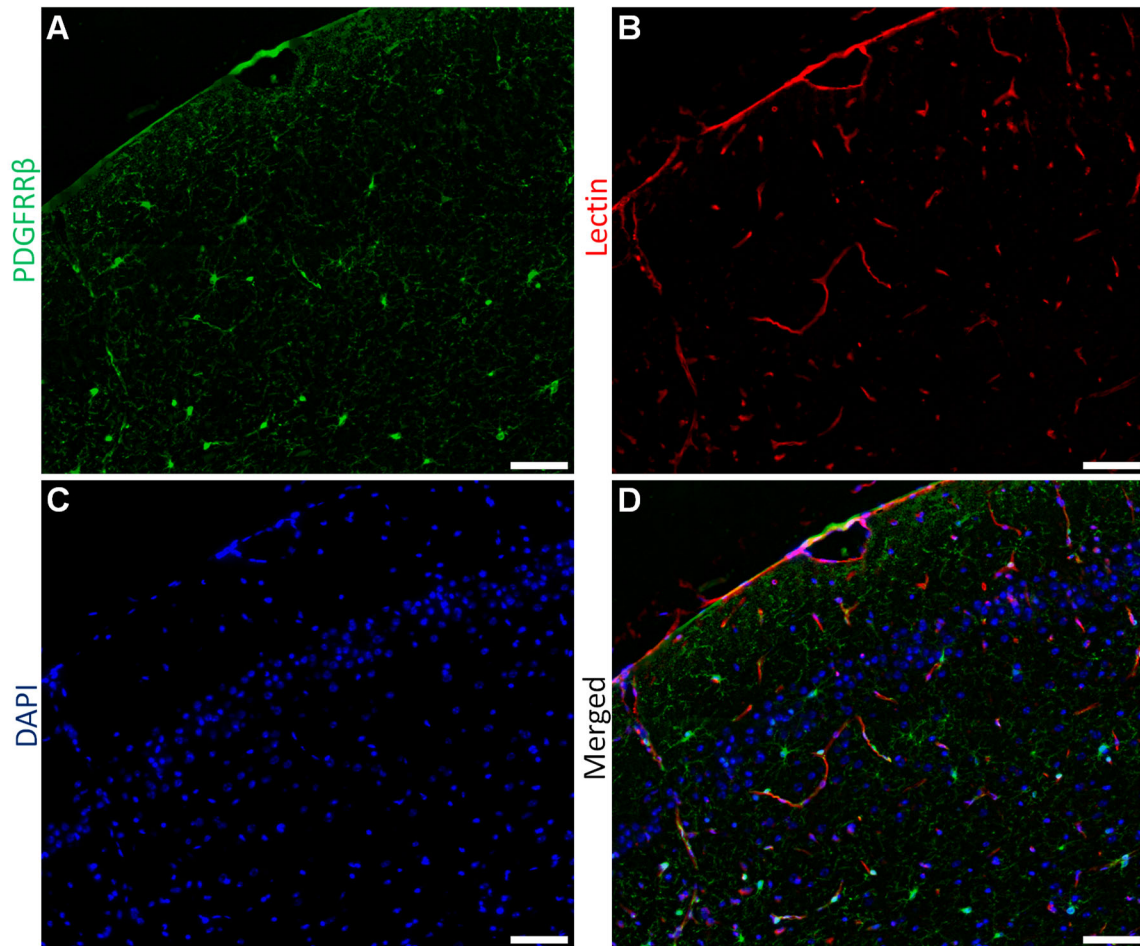


**Figure S4. Representative pericyte and endothelium labelling in peri-ischemic tissue.**



Tissue was perfusion-fixed at the 24h follow-up and pericytes and endothelium labelled with platelet derived growth factor receptor  $\beta$  (PDGFR $\beta$ ; **A**; green), and lectin (**B**; red), respectively; and nuclei highlighted with 4',6-diamidino-2-phenylindole (DAPI; **C**; blue). **D**, Spatial relationships of the three labels are shown in the triple merged image. Bars, 100  $\mu$ m. See Fig. 7 for statistical analysis.

**Video S1. Laser speckle contrast imaging during arterial occlusion.** Laser speckle contrast imaging ensured no-flow in the targeted artery during the 1h occlusion. The top left panel shows absolute blood flow index (BFI) in each pixel. The top right panel shows overlay of BFI values at the given time point relative to baseline. Only BFI changes exceeding the threshold of  $\pm 25\%$  are overlaid as specified by the color bar on the right side to show relevant BFI changes. Relative changes in blood flow (right panel) show the drop in blood flow downstream from the targeted artery. The baseline in the right panel is reset at 4 minutes and 10 seconds (as indicated 10 seconds into the video) to highlight the changes in BFI after the first spreading depolarization (SD). Multiple spreading depolarizations propagated through the peri-ischemic cortex during the arterial occlusion. This was associated with a drop in BFI in the peri-ischemic cortex. The bottom panel presents mean BFI over time in the three corresponding color-coded regions of interest.

**Video S2. Increased capillary flow stalling after reperfusion.** Capillary flow stalling was assessed by optical coherence tomography angiograms. Representative angiograms are shown at baseline (left) and 3h after reperfusion (right). Capillary flow stallings as indicated with arrows.

**Video S3. Rhythmic and synchronized capillary flow stalling.** In one mouse, a group of capillaries showed rhythmic stalling with a frequency of approximately 0.1 Hz. Capillary flow dynamics were assessed by optical coherence tomography angiography. Video speed x30. Stalling data from this mouse is shown in Figure S3, indicated Mouse #1.